2017

Mode Evolution in Fiber Based Devices for Optical Communication Systems

Bin Huang
University of Central Florida

MODE EVOLUTION IN FIBER BASED DEVICES FOR OPTICAL COMMUNICATION SYSTEMS

by

BIN HUANG
B.S. Applied Physics, East China University of Science and Technology, 2011
M.S. Optics and Photonics, University of Central Florida, 2013

A dissertation submitted in partial fulfillment of the requirements
for the degree of Doctor of Philosophy
in CREOL, the College of Optics and Photonics
at the University of Central Florida
Orlando, Florida

Fall Term
2017

Major Professor: Guifang Li

ABSTRACT

Space division multiplexing (SDM) is the most promising way of increasing the capacity of a single fiber. To enable the few mode fiber (FMF) or multi-mode fiber (MMF) transmission system, several major challenges have to be overcome. One is the urgent need of ideal mode multiplexer, the second is the perfect amplification for all spatial modes, another one is the modal delay spread (MDS) due to group velocity difference of spatial modes. The main subject of this dissertation is to model, fabricate and characterize the mode multiplexer for FMF transmission. First, we designed a novel resonant mode coupler (structured directional coupler pair). After that, we studied the adiabatic mode multiplexer (photonic lantern). 6-mode photonic lantern using graded-index (GI) MMFs is proposed and demonstrated, which alleviates the adiabatic requirement and improves mode selectivity. Then, 10-mode photonic lantern is demonstrated using novel double cladding micro-structured drilling-hole preform, which alleviates the adiabatic requirement and demonstrate a feasible way to scale up the lantern modes. Also, multi-mode photonic lantern is studied for high order input modes. In addition, for the perfect amplification of the modes, cladding pump method is demonstrated. The mode selective lantern designed and fabricated can be used for the characterization of few mode amplifier with swept wavelength interferometer (SWI). Also, we demonstrated the application of the use of the few mode amplifier for the turbulence-resisted preamplified receiver. Besides, for the reduction of MDS, the long period grating for introducing strong mode mixing is demonstrated.

To my advisors and friends

ACKNOWLEDGMENTS

To explore the fields of mode evolution in fiber based device is an absolutely amazing experience. I truly appreciate my advisors Dr. Guifang Li in CREOL and Dr. Nicolas Fontaine and Dr. Haoshuo Chen in Bell Labs for the great journey. My advisor Dr. Li provides me the best to help me grow even in the times when his funding was tight. Without him, I cannot go that far. Working under Dr. Fontaine is one of the greatest times in my life. Dr. Chen is both a tutor and a friend. I am greatly indebted to them and hopefully I can return the favor one day. Also, I would like to thank Dr. Rodrigo Amezcua Correa and Dr. Roland Ryf for the guidance and Dr. Ayman Abouraddy to be as my committee member.

I would like to thank all the former and current members of the OFC group and beyond for their help and discussion. Dr. He Wen gave me a lot of help and guidance in various fields. Dr. Neng Bai guided me through the realm of mode division multiplexing. Dr. Cen Xia and I had more than three years overlap, we both experienced the success and failure of projects in space division multiplexing. Huiyuan Liu and I worked together in various projects. Christian and I worked together on the preamplified few mode receiver and we showed good teamwork. Dr. Binbin Guan is a fun and nice guy and he gave me several useful advices and guidance. Dr. Jin Cang brought all kinds of fibers for us to explore and he has good personality. I would also like to thank my roommate and workmate Dr. Kuanping Shang for the mutual effort on cladding pumped amplifiers.

Last but surely not least, I would like to thank my parents for their unlimited support. Special thanks to my uncle for great guidance through my life.

TABLE OF CONTENTS

LIST OF FIGURES

LIST OF TABLES

LIST OF ACRONYMS AND ABBREVIATIONS

Acronyms/Units	Descriptions
AO	Acoustic optics
Demux	De-multiplexer
DSP	Digital signal processing
EDF	Erbium doped fiber
EDFA	Erbium doped fiber amplifier
FMF	Few- mode fiber
FSO	Free space optics
GI	Graded - index
HOM	Higher-order mode
IL	Insertion loss
MCF	Multi-core fiber
MDG	Mode dependent gain
MDL	Mode dependent loss
MDM	Mode division multiplexing
MDS	Modal delay spread
MGS	Mode group selective
MIMO	Multiple-input multiple-output
MMF	Multi-mode fiber
Mux	Multiplexer
PL	Photonic lantern

QAM	Quadrature amplitude modulation
QPSK	Quadrature phase shift keying
SDM	Space division multiplexing
SMF	Single-mode fiber
SNR	Signal noise ratio
SSMF	Standard single-mode fiber
WDM	Wavelength division multiplexing

CHAPTER 1: INTRODUCTION

Optical fiber communication is the backbone for the telecommunications infrastructure that supports the internet. As the internet demand keeps on increasing, the need for a single fiber to carry more information is crucial. It is very important to find smart solution to increase the capacity x times in a single fiber by increasing the cost much less than x times. That criterion was explored extensively by a large number of researchers. The capacity for a single fiber increases by a factor of 10 every 4 years. The capacity improvement includes improved transmission fibers, the use of wavelength division multiplexing (WDM) [1,2] and Erbium doped fiber amplifier (EDFA) [3–5] and recently the high spectral efficiency coding [6,7]. The transmission fiber has been improved greatly, so far the loss of single mode fiber (SMF) is as low as 0.015 dB/km [8]. The achievement of low loss can greatly increase the span length before it gets amplified by the EDFA. To have a more clear understanding of the significance of the low loss benefit, we take an example. One fiber has 0.02 dB/km loss and the other one has 0.2dB/km loss. If the amplification is 15dB, the maximum span length for fibers with 0.02dB/km loss can be 75km, while for fibers with 0.2 dB/km, the span length can only be 7.5 km. That is 10 times difference! Now the loss mainly comes from the fundamental limit of scattering [9]. Further improvement of fiber loss can be difficult due to that fundamental limit. EDFA and WDM enable the utilization of various wavelength channels. The demonstration of EDFA has the great advantage of large gain and low noise figure, which greatly increase link transmission distance. In addition, EDFA can amplify a large bandwidth of signals simultaneously. With the arrival of WDM, a large number of wavelength channels can be launched into a single fiber. The sharing of amplification of wavelength channels could dramatically increase the capacity per fiber with much less cost increase. With the utilization of both WDM and EDFA, the capacity increase can be more than 2 orders of magnitude per single fiber.

Another improvement is the high spectral coding with the availability of coherent receiver. The signal can be modulated with multi-level phases, for example, quadrature phase-shift keying (QPSK), which has four phase states for a single pulse. That means for single pulse can carry 2 bits. By the same token, 16 quadrature amplitude modulation (QAM) and 64 QAM can achieve 4 and 6 bits per single pulse. For undersea long-haul transmission applications, QPSK signal with coherent detection has been widely used [10].

These improvements are based on single mode fiber transmission. Further improvement is difficult, since the recent progress has already close to the Shannon's capacity limit which can be expressed as $C = Wlog(1 + SNR)$ where W is the bandwidth of the channel and SNR represents the signal-to-noise ratio. As current system has already exhausted all degrees of freedom, namely quadrature, wavelength channel and polarization plus the good quality low loss optical fiber. The only dimension not taken into consideration is the spatial modes. As we know, SMF has two vector modes (one spatial mode), each vector mode can carry independent information. Single fibers with modes more than 2 are termed as space division multiplexing (SDM) fibers. SDM fibers can be categorized as few-mode fibers (FMFs) or multi-mode fibers (MMFs), multi-core fibers (MCFs) and multi-element fibers. FMFs (MMFs) and MCFs are very promising candidates for the improvement of fiber capacity. We will discuss them in the following.

1.1. Few-mode fibers for space division multiplexing

Few-mode fibers have a larger core size than single mode fiber, thus it can support high-order modes. As shown is Figure 1.1, we draw a step-index fiber with increasing core diameter. The refractive index of the core is n_1 and the index of the cladding is n_2 ($n_1 > n_2$). We use a parameter V to get implication of the number of modes. The V number is defined as $V = \frac{2\pi}{\lambda} a\sqrt{{n_1}^2 - {n_2}^2}$

where λ is the wavelength and a is the radius of the fiber core radius. At the beginning, the core size is small, it can only support the fundamental spatial mode (2 vector modes). We call it LP_{01}. We use the linear polarization (LP) basis which is more convenient without degrading the rigor of the analysis in the following chapters. As the core size becomes larger, V number also increases. When V number becomes more than 2.405, the fiber becomes a few-mode fiber. At 2.405<V<3.8, the fiber can support two more spatial modes (four vector modes), LP_{11a} and LP_{11b}.

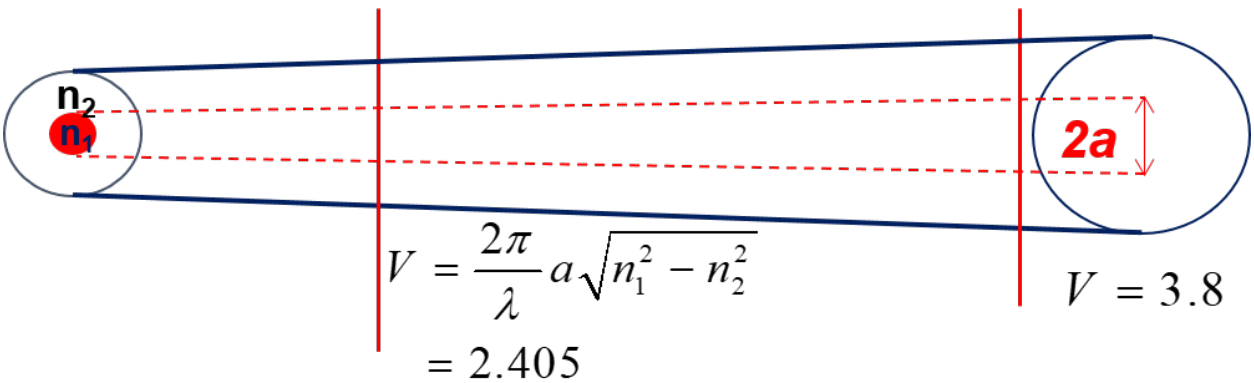

Figure 1.1 Transition from single mode fiber to few mode fiber by increasing the core diameter.

As the core diameter further increases, the fiber can support more and more spatial modes. If a fiber can support N spatial modes, then the potential capacity of this fiber can be N times than the SMF. The mode scalability N can be very large, up to more than 100 spatial modes with the same 125 μm as SMF. As the first step, we investigated the FMFs, which by convention can support the modes much less than 50 spatial modes. Tremendous efforts have been taken for the exploration of the potential advantages of transmitting signals in FMFs [11–16]. Figure 1.2 shows SDM fiber transmission system. N independent information channels from N transmitters (Txs) are combined by N x N spatial multiplexer (Mux) into the SDM fiber. The role of the spatial Mux is to map all the modes from SMFs to the modes of SDM fiber with no information loss. During

transmission, the signals are amplified simultaneously by the SDM amplifier which requires the equalized amplification of all the modes. At the receiver, the signals are demultiplexed by the spatial demultiplexer (DeMux) and recovered through multiple-input multiple-output (MIMO) digital signal processing (DSP).

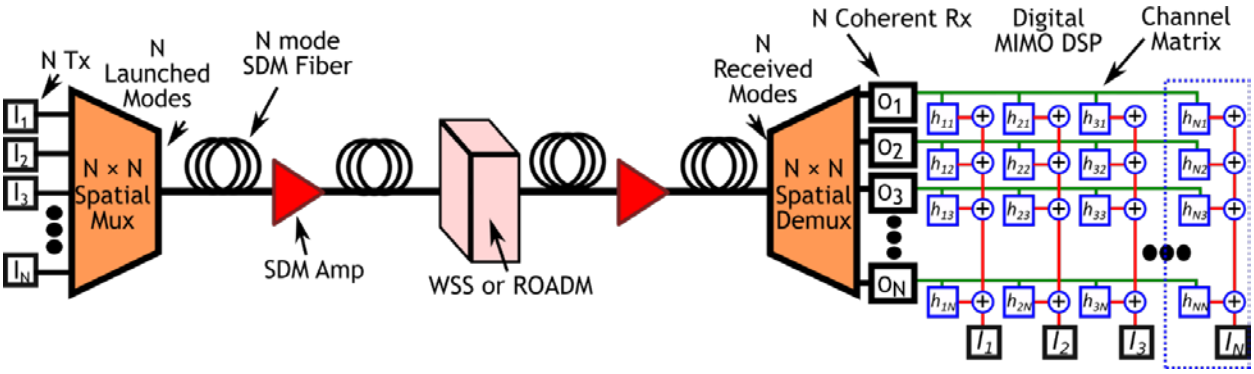

Figure 1.2 Schematic for SDM transmission system

However, transmission using few-mode fiber has some difficulties to overcome. There are in general three big challenges. The first is how to launch all the spatial modes carrying independent information into the few-mode fiber. The transmitter nowadays is single mode based, thus it poses big difficulties to launch spatial modes. Low mode dependent loss (MDL) and insertion loss (IL) mode Muxes are crucial to solve this problem. This is the major problem this thesis tries to tackle. The second challenge comes from the mode dependent gain (MDG) from the few-mode amplifier. The amplification of all spatial modes is performed in one few-mode amplifier. The gain of each spatial mode can be different, which is determined by the overlap of intensity profile of the spatial mode and pump light intensity profile on Erbium dopants. MDG would lead to capacity loss. The third challenge is the nature that modes propagate at different speed and modes weakly couple to each other during transmission, which would lead to a long modal delay spread at the coherent receiver. The complexity would be too large for the DSP to recover the signals. One effort

to reduce modal delay spread (MDS) is to use graded-index (GI) FMFs to replace SI SMFs. For the same number of modes, the MDS of GI FMFs has much shorter MDS than SI FMFs more than 10 times [17–19]. The spatial modes in GI FMFs can be divided into mode groups. Spatial modes within the mode group has almost same effective index and very close modal group delay (MGD). In addition, modes within the mode group have strong crosstalk during fiber transmission. For modes belong to different mode groups, they have different effective indexes and MGDs. The crosstalk between them is weak but cannot be neglected. We have typical few mode GI fibers supporting 3 modes (2 mode groups), 6 modes (3 mode groups), 10 modes (4 mode groups) and so on.

The 3 challenges must be tackled before FMFs can be used for the replacement of SMFs.

1.2. Multi-core fibers for space division multiplexing

MCFs are another promising SDM fibers, which has multiple cores shared by the same cladding. MCFs can be divided into two categories, uncoupled-core MCFs [20–27] and coupled-core MCFs [28–32]. Uncoupled-core MCFs in essence are simply SMFs sharing the same core. The distance between the cores is large enough (more than 40 μm) so that the crosstalk between neighboring cores is negligible, which in theory can achieve same performance as SMFs. The capacity can be more than 10 times than SMFs. The cost per bit margin of uncoupled-core MCFs over SMFs is not significant, since these two fibers are the same in physics. However, uncoupled-core MCFs do have certain advantages over SMFs, which is the compactness. The volume per mode of uncoupled-core MCFs over SMFs makes uncoupled-core MCFs promising in the application of data center connection [33].

Coupled-core MCFs have smaller core to core distances, usually less than 20 μm. The coupling between the neighboring cores can be strongly coupled to each other, which leads to significant advantages over SMFs. The big advantage over SMFs is reduced nonlinear impairment due to strong crosstalk. The capacity increase can be more than 20s compared to SMFs. The only penalty for coupled-core MCFs is the requirement of MIMO DSP at the receiver. The receiver complexity is directly related to the delay spread of the coupled-core MCFs, which is related to the core to core distance. We demonstrated that 17.5 μm core to core distance would lead to smallest delay spread [34].

1.3. Dissertation Outline

In this dissertation, the main focus is on tackling the challenges in FMF transmission. The main effort is on the multiplexer for SDM. In addition, we demonstrate ways to introduce low MDG amplifiers and its new application in free space optical (FSO) communication and demonstrate mechanical grating for strong mode mixing to reduce MDS. CHAPTER 2: provides introduction to resonant mode coupler and the work of directional coupler pair for mode Mux. CHAPTER 3: discusses the adiabatic mode Mux (photonic lantern) and a novel way for 6 mode photonic lantern which greatly reduce adiabatic requirement. CHAPTER 4: discusses the proposal and demonstration of 10 mode photonic lantern using novel drilling-hole preform for further reducing adiabatic requirement. CHAPTER 5: presents studies of cladding pumped low MDG amplifier, gain characterization using photonic lanterns and its application in FSO communication. CHAPTER 6: presents studies of the use of mechanical grating for mode mixing for few mode fiber transmission. Chapter 8 gives conclusions of this dissertation and discusses possible future research.

CHAPTER 2: RESONANT MODE MULTIPLEXER

The resonant mode converter has been widely explored in applications of areas other than SDM transmission [35–41]. The resonant mode converters include long-period grating [37–41] and directional coupler [35,36]. The most basic mechanism of long-period grating and directional coupler is the effective index matching, which resonantly couples one mode to the targeted mode with very low loss.

For mode MUX applications, we have additional requirement, since the mode MUX requires the fundamental modes from SMFs be converted to each spatial modes in FMF with low MDL and IL. In addition, we have one more criterion to follow for FMF long haul transmission, which is all the spatial modes converted must fully fill the modes FMF can support. For example, a 3-mode fiber can support LP_{01}, LP_{11a} and LP_{11b}. By launching only LP_{01} and LP_{11a} is not enough, since LP_{11a} and LP_{11b} will couple to each other during transmission, leading to capacity loss. Long-period grating for this application is not suitable. Although it can convert the fundamental mode to any desired spatial mode, the lack of the ability to combine the converted mode together makes it not suitable as mode MUX. The directional coupler has the potential, since it can couple the fundamental mode of a single-mode fiber to a high-order mode of a FMF if the propagation constants of the said modes are substantially the same. However, there is one major obstacle, that is for few-mode fiber, we have degenerate spatial modes, like LP_{11a}, LP_{11b} and LP_{21a}, LP_{21b}. Those modes rotates and mixes in short distance. One proposed way of realizing independent excitation of degenerate modes using fiber-based direction couplers is to make the multimode fiber elliptical rather than circular [42]. However, elliptical fibers are harder to make and they are not compatible with the circular MMFs used for optical transmission systems. We

propose here a method for multiplexing and demultiplexing degenerate mode using structured directional coupler pairs.

2.1. Structured Directional Coupler Pair

Figure 2.1 illustrates an example of the structured directional coupler pair. For simplicity, we assume the fibers are step-index fibers. The FMF (fiber 1) has a core and cladding radius of a_1 and r_1, respectively. The SMFs (fiber 2 and fiber 3) have core and cladding radius of a_2 (a_3) and r_2 (r_3), and length of L_2 (L_3), respectively. The orientation of the fibers are such that the angle subtended by the lines from the center of the FMF to the centers of the SMFs is φ. We use the multiplexing of the lowest-order degenerate LP_{11a} (vertically oriented) and LP_{11b} (horizontally oriented) modes as an example. Multiplexing of higher-order degenerate modes will be similar. If we design the fiber index and core radius so that propagation constants of the LP_{11a} and LP_{11b} modes of the FMF and that of the fundamental mode of each of the SMFs are the same, the coupled-wave equations for the amplitudes of the four spatial modes are given by

$$\frac{d}{dz}\begin{bmatrix} A_2 \\ A_{11a} \\ A_{11b} \\ A_3 \end{bmatrix} = j\begin{bmatrix} \beta & c_1 & 0 & 0 \\ c_1 & \beta & 0 & c_1\cdot\cos\varphi \\ 0 & 0 & \beta & c_1\cdot\sin\varphi \\ 0 & c_1\cdot\cos\varphi & c_1\cdot\sin\varphi & \beta \end{bmatrix}\begin{bmatrix} A_2 \\ A_{11a} \\ A_{11b} \\ A_3 \end{bmatrix} \tag{2.1}$$

where the coupling coefficients in the coupling matrix are given by

$$c_1 = \frac{\omega\varepsilon_0 \int_{-\infty}^{+\infty}\int_{-\infty}^{+\infty} (N^2 - N_2^2) E_{11a}^* E_2 \, dxdy}{\int_{-\infty}^{+\infty}\int_{-\infty}^{+\infty} u_z (E_{11a}^* \times H_2 + E_{11a} \times H_2^*) dxdy},$$

of the extended core-to-core distance, waves in the two single-mode fibers do not couple to each other. The degenerate modes LP_{11a} and LP_{11b} are orthogonal to each other and are exactly the same if one degenerate mode is rotated by 90°. As a result, for the special case of $\varphi = 90^o$, the SMFs can be positioned in a way such that single-mode core 2 only couples to the LP_{11a} and single-mode core 3 only couples to the LP_{11b}.

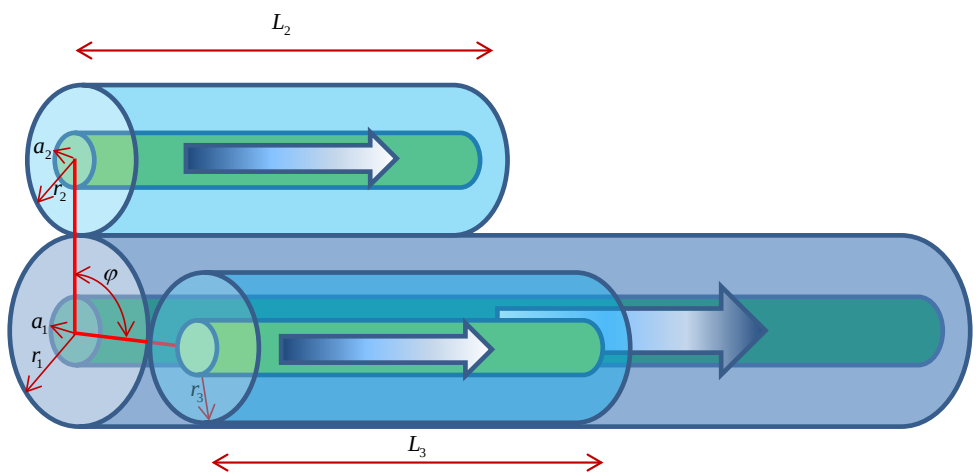

Figure 2.1 Structured directional coupler pair for mode MUX

Based on that, we proposed a design for multiplexing and demultiplexing 3-spatial mode. In our design, the core radius of the FMF (fiber 1) is designed to be $10\mu m$ and the core-cladding index difference is 0.004 at wavelength $1.55\mu m$. The modes supported by the FMF are up to the degenerare LP_{21} modes. The two silica step-index SMFs are designed to be identical with core radius $3.5\mu m$ and the same core-cladding index difference, which is so designed that the effective index matches that of the LP_{11} mode (1.4459). Figure 2.2 illustrates the evolution of the field amplitude, simulated using the beam propagation method, in the structured directional coupler pair when the inputs in the two single-mode fibers are in phase, out of phase and in quadrature. The residual intensity is at least -20 dB down from the excited LP_{11} mode. The output fields in the FMF

are the $+45^0$ LP_{11}, -45^0 LP_{11} and the right-handed vortex LP_{11} modes, respectively. This clearly demonstrates the ability of the structured directional pair to generate the complete basis functions for the degenerate LP_{11} modes. Therefore, the signals in the two SMFs connected to two independent single-mode transmitters will be coupled to the two degenerate modes LP_{11a} and LP_{11b}. The launch of the fundamental mode can be achieved by splice SMF to the FMF directly.

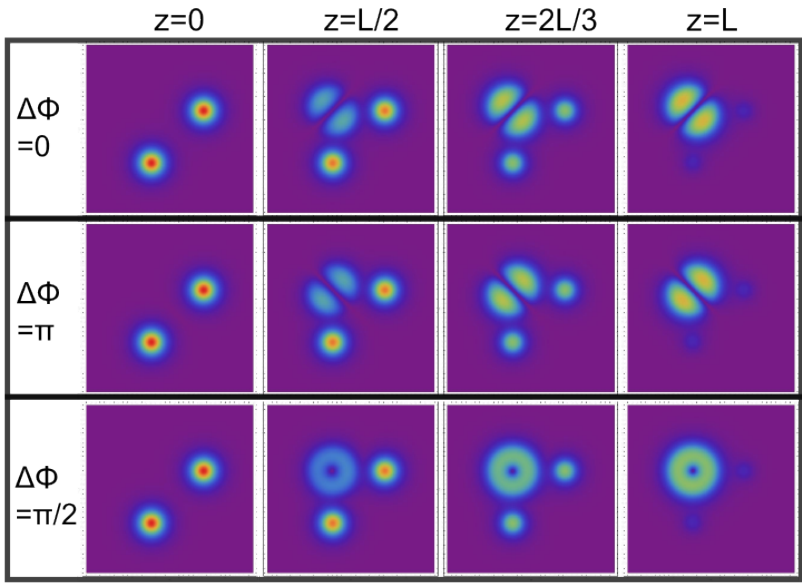

Figure 2.2 Evolution of the magnitude of the field at several distances in the coupling reason for in phase, out of phase and quadrature excitation.

Figure 2.3 shows the coupling efficiency of the directional coupler pair for the degenerate LP_{11} modes as a function of wavelength in the C band optimized for 1550nm. It is found that when core to core distance is small, the bandwidth of the coupler can cover C band.

In general, the structural directional coupler pairs can be cascaded as mode selective Mux for arbitrary many spatial modes. Figure 2.4 shows the schematic of the cascaded directional coupler pairs. In that figure, up to 6 spatial modes can be multiplexed. Since each mode excited at the coupler pair is converted to a unique spatial mode of the FMF, the coupling matrix is diagonal.

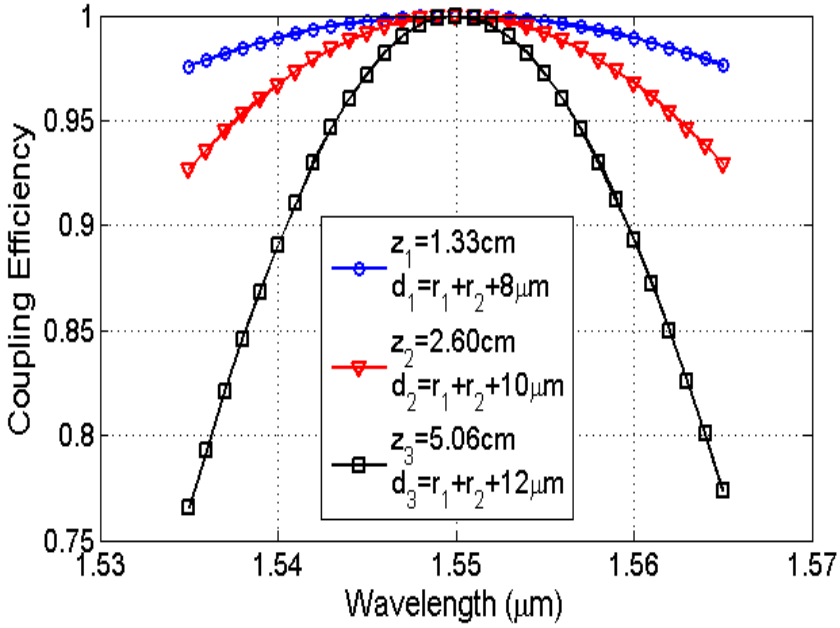

Figure 2.3 Coupling efficiency of directional coupler pair for LP_{11} vs wavelength

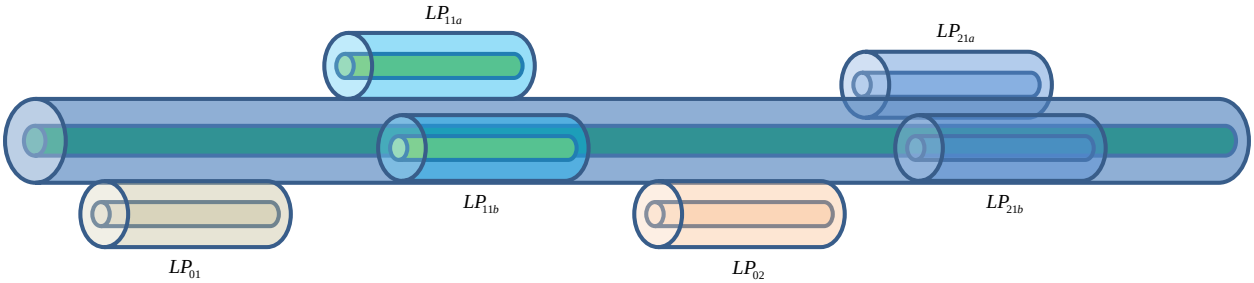

Figure 2.4 Cascaded directional coupler pairs of mode Mux

CHAPTER 3: PHOTONIC LANTERNS USING GRADED-INDEX FEW-MODE FIBERS

Fiber-based photonic lanterns (PLs), in which multiple optical fibers are adiabatically transformed into a single MMF, are a promising candidate for mode Muxes as they have low insertion loss (IL) and low mode dependent loss (MDL) if the PL is adiabatically tapered and packed optimally [43–47]. Also, the bandwidth of the PLs can be very broad compared to directional coupler pairs [48] whose bandwidth is limited by the phase-matching condition. The only physics requirement for the PL is the mode evolution has to be adiabatic across the broad bandwidth.

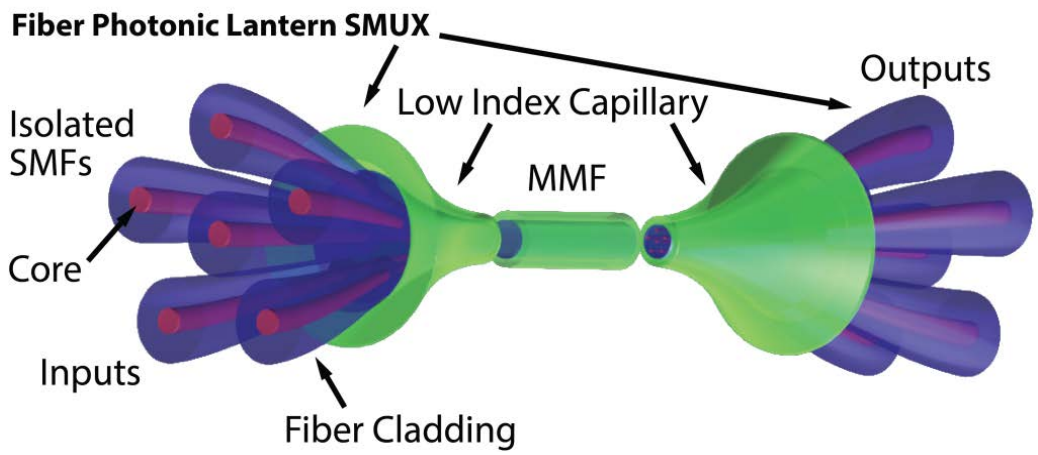

Figure 3.1 Schematic of photonic lantern based mode Mux (DeMux)

The structure of a photonic lantern is shown in Fig. 3.1. A PL-based multiplexer consists of M individual fibers with a core of index $n_{2,m}$ and core diameter r_m surrounded by a cladding with refractive index $n_{1,m}$ that are packed into a capillary made of fluorine-doped silica with a refractive index n_0 that is lower than the fiber cladding. The packing geometry is not arbitrary and it must follow certain geometry [49]. The entire structure is then adiabatically tapered. During the

taper, light that is initially confined in the individual cores escape the cores as the cores shrink. The escaped light is captured and guided by the cladding and low-index capillary. At the end of the taper, each core is so small that they have little effect on the output modes of the PL, and the light is then guided by the core made of the fiber cladding material with the low-index capillary as the new cladding. When the individual fibers are identical, $n_{2,i} = n_{2,j}$ and $r_i = r_j$, the PLs are typically non-mode selective. Launching light into any individual fiber core will excite a combination of modes at the lantern output which is decided by the structural geometry of the PL. Mode-selective lanterns can be made if $n_{2,i} \neq n_{2,j}$ and/or $r_i \neq r_j$ for each mode. Similarly mode group selective (MGS) lanterns can be made if $n_{2,i} \neq n_{2,j}$ and/or $r_i \neq r_j$ for each mode group. Dissimilar fibers break the degeneracy of the local modes of the lantern throughout the entire taper and force each input core to map to each mode of the output MMF. Symmetry can be selectively preserved for degenerate modes in the same mode group of the output fiber of the PL. For FMF transmission, modes in the same mode group couples strongly, thus mode MGS-PL is of interest. Demonstrations of a MGS-PL for the LP_{01}LP$_{01}$ mode (1st mode group) and the LP_{11}LP$_{11}$ modes (2nd mode group) have verified this concept [45]. A SMF with a higher effective index was mapped onto the LP_{01} output mode and two SMFs with a lower effective index were mapped onto the LP_{11} output mode group.

The ability for the PL to scale to more mode groups is very desirable for high-capacity SDM transmission systems. Theoretically for MGS-PLs, there is no restriction in terms of scalability, provided that the adiabaticity criterion is satisfied in the taper transition, given by [50]:

$$\left| \frac{2\pi}{\beta_1 - \beta_2} \frac{d\rho}{dz} \int \psi_1 \frac{\partial \psi_2}{\partial \rho} dA \right| << 1 \tag{3.1}$$

where Ψ_1 and Ψ_2 are the normalized field distribution of the local modes that are likely to couple to each other, β_1 and β_2 are their respective propagation constants, ρ is the local core radius, z is the longitudinal distance along the PL, A is the cross-sectional area of the PL. The first term of Eq. (3.1) dictates that the tapering rate $\frac{d\rho}{dz}$ is inversely proportional to the differences in the propagation constants of the two modes (i.e., propagation constant criterion). The second terms of Eq. (3.1) suggests that mode profiles that change slowly as the fiber is tapered will lead to low crosstalk (i.e., mode profile criterion). It was argued in [50] that each of these two effects requires tapering length to increase linearly with N and therefore the combined effect requires the tapering length to increase approximately as N^2. In [50], reduced-cladding SMFs, which has much slower change of the mode field diameter as it is tapered, was used to satisfy the adiabaticity requirement via the mode profile criterion.

We proposed methods to alleviate the adiabatic requirement and demonstrated PLs with these improvements experimentally.

3.1. Rationale of Photonic Lanterns using Few-mode Fibers

We propose to use GI-MMFs as the input fibers instead of SMFs to satisfy the adiabatic requirement via both the propagation constant criterion and the mode profile criterion. To improve the propagation constant criterion, large difference of $(\beta_1 - \beta_2)$ will greatly reduce the adiabaticity requirement. Dissimilar MMFs as input fibers offer a much larger range of propagation constant differences between their fundamental modes than what dissimilar SMFs allow. Propagation constant differences between dissimilar SMFs are constrained by the available core diameter and refractive index to maintain single-mode operation. To improve the mode-profile criterion, we use

GI-MMFs because the mode changes slower than that of the step-index MMF, which will be discussed in the following paragraph.

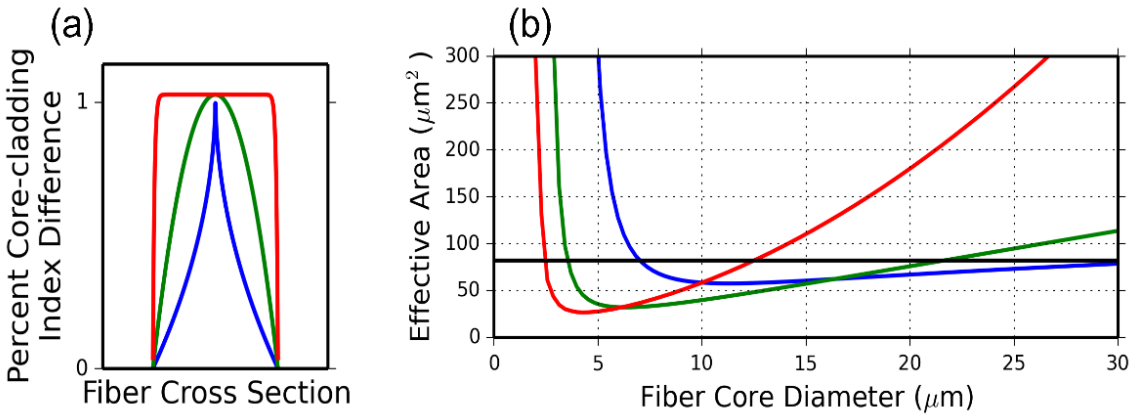

Figure 3.2 (a) Refractive index profile of MMFs. Step index MMF (red), $\alpha = 2$ graded index MMF (green), $\alpha = 0.5$ graded index MMF(blue). (b) Effective area of the fundamental mode of different fibers in the taper. Step index MMF (red), $\alpha = 2$ graded index MMF (green), $\alpha = 0.5$ graded index MMF(blue). The black line represents the effective area of SSMF (80 μm²).

The use of multimode fiber for the input/output PL is practical for two reasons. First, when the length of the MMF is short, mode coupling between different spatial modes of the MMF is negligible. Second, standard SMFs (SSMFs) can be coupled to the fundamental mode of GI-MMFs with low splice-loss even if the diameter of the dissimilar GI-MMFs varies. The effective area of the fundamental mode of the GI-MMF can be designed to be approximately equal to SSMF for a wide range of core diameters. Figure 3.2(a) shows the refractive index profile of three types of MMFs [step-index MMF (red), GI-MMF with $\alpha = 2$ (green) and $\alpha = 0.5$ (blue)]. Figure 3.2 displays the effective areas of the fundamental mode of these fibers as a function of core diameter. The core-cladding index contrast is set to 1%. From Figure 3.2 (b), two advantages of GI-MMF compared to step-index MMF are apparent: 1) the effective area of the GI-MMFs changes much slower than step-index MMFs as the core diameter varies which better satisfies the mode-profile

criterion, and 2) the effective area of GI-MMF with $\alpha = 2$, almost matches the SSMF (80μm²) over a wide range of core diameters between 15 μm and 25 μm, which results in low splice loss. Changing α and the core-cladding index contrast can further optimize the splice loss between GI-MMFs and the external SSMF. Finally, GI-MMFs with 125 μm claddings are easier to handle than reduced cladding fibers.

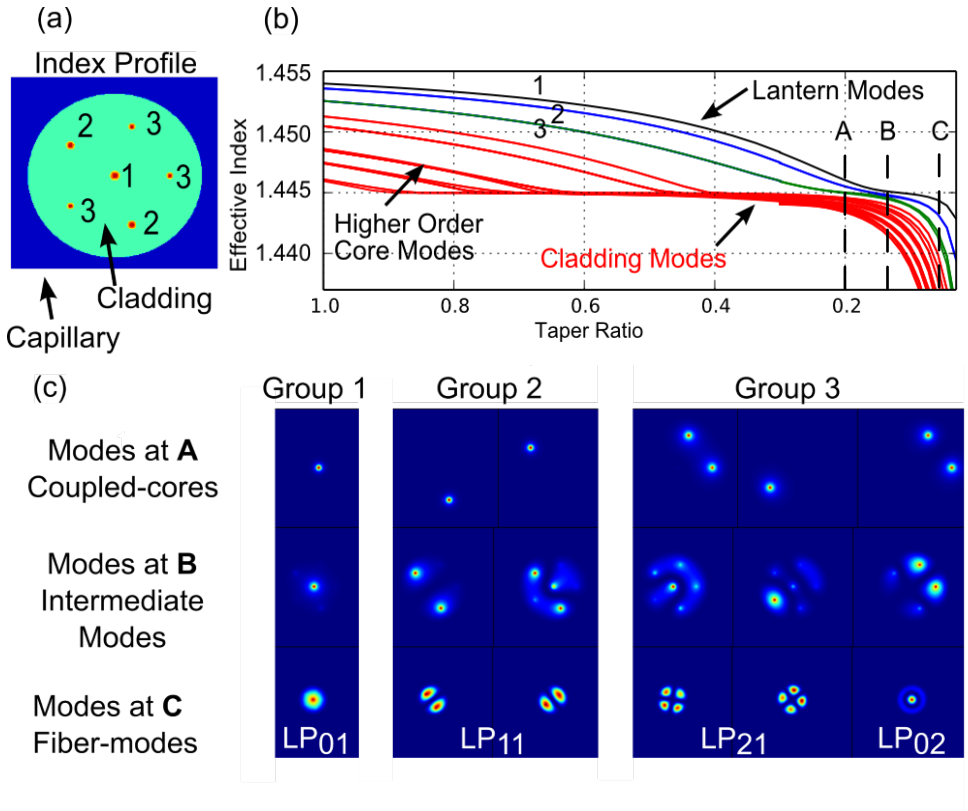

Figure 3.3 (a) Six-mode lantern index profile with 3 types of dissimilar cores (1, 2 and 3) (b) effective indexes vs taper ratio and (c) intensity of the modes at different stages of the taper.

From discussions above, selection of dissimilar GI-MMFs is critical to building a MGS-PL. The selection rules are two-fold. First, the difference of propagation constants between fundamental modes corresponding to the output mode groups should be as large as possible to make adiabatic tapering robust. For MGS PLs using GI-MMFs, the fundamental mode launched into an

individual core maps to the corresponding lantern mode, while higher order modes in an individual core couple to the cladding modes (guided by the capillary) that eventually becomes radiative.

Figure 3.3 shows a simulation using input fibers that meet those selection rules for a three mode group MGS-PL. Figure 3.3(a) shows the fiber cross section. The input fiber at the center is a 22μm-core-diameter GI-MMF for exciting the LP_{01} output mode (group 1), the two 20μm-core-diameter GI-MMFs excite the two LP_{11} modes (group 2) and the three 15μm-core-diameter GI-MMFs excite the three nearly-degenerate LP_{21} + $LP_{01}\mathrm{LP}_{21} + \mathrm{LP}_{02}$ modes (group 3). The index contrast of the GI-MMF in the simulation is 1%. The claddings have diameters of 125μm. In Figure 3.3 (b), the effective indexes of the 3 mode groups of interest (1-black, 2-blue, 3-green) and other higher order mode groups (red) of the individual fibers that become cladding modes are plotted as functions of the taper ratio. It is noted that the effective index of the higher-order modes are smaller than that of any of the fundamental modes of the 6 dissimilar fibers, ensuring no resonant coupling occurs between a high-order mode from one input fiber to a fundamental mode of another fiber. Another constraint is that the effective index of the modes should not cross or interact with each other during the taper. To be more specific, the effective index of the fundamental mode of each GI-MMF must be larger than that of any higher order mode in any of the input fibers.

At a taper ratio around 0.9, the highest-order modes of each fiber begin to couple to the cladding modes (guided by capillary). At a taper ratio around 0.4, all the higher order modes evolve to the modes guided by the capillary, while the fundamental modes are still guided by individual cores. Geometric requirement ensures that the effective indexes of any higher-order mode were smaller than that of one of the fundamental modes during the tapering shown in Figure 3.3(b).

Figure 3.3(c) depicts the intensity patterns of the PL modes at different points in the taper region. For taper ratios from 1 to 0.2 (region before A), the cores are brought closer together but

the lantern modes are still well confined within the GI-MMF cores. At B (taper ratio=0.15), the mode escapes the individual core and becomes guided by a combination of cores. At C (taper ratio around 0.11), the cores become small enough that the PL modes appear in the MMF composed of the fused-cladding core and capillary cladding. After C, the cores become so small that they have negligible effect on the PL modes and the structure can be tapered to desired dimensions. The transition between A and C (especially around B) is the most sensitive because the mode profiles change significantly as the photonic-lantern modes transition from core-guiding and cladding-guiding. As a result, the taper speed in fabrication could be fast for taper ratios from 1.0 to A and should be slow between points A and C.

3.2. Fabrication and Characterization of Photonic Lantern

Table 3.1 shows detailed construction of GI-MMF-based MGS-PL supporting 2 and 3 mode groups. The GI-MMFs are selected such that the effective indices between the fundamental mode and the higher order modes do not cross. Figure 3.4(a) and (b) show the end facet and the near-field output mode intensity profiles of the fabricated two mode group MGS-PL. High modal selectivity is observed between these two mode groups. As expected, for the degenerate LP_{11}LP$_{11}$ mode groups, a ring-like intensity profile representing linear combination of the two LP_{11}LP$_{11}$ modes exhibits high selectivity to LP_{01}LP$_{01}$ mode. Figure 3.5(a) and (b) show the end facet and near-field output intensity profiles of a three mode group MGS-PL. Three mode groups can be clearly observed. The tapered end of the PL is butt coupled to a 50-μm core diameter GI-MMF. Figure 3.4(c) and Figure 3.5(c) show the output field at the end of a 50-m GI-MMF which indicates qualitatively that the desired mode groups have been excited using the MGS-PLs.

Table 3.1 Parameters of mode group selective lanterns

	2-mode group selective lantern	3-mode group selective lantern
Fiber for LP_{01} mode (mode group 1)	20μm GI-MMF	22μm GI-MMF
Fiber for LP_{11} modes (mode group 2)	15μm GI-MMF	20μm GI-MMF
Fiber for $LP_{21} + LP_{02}$ modes (mode group 3)		15μm GI-MMF
Taper Ratio	8.5	11.2
Final Diameter	27μm	29μm

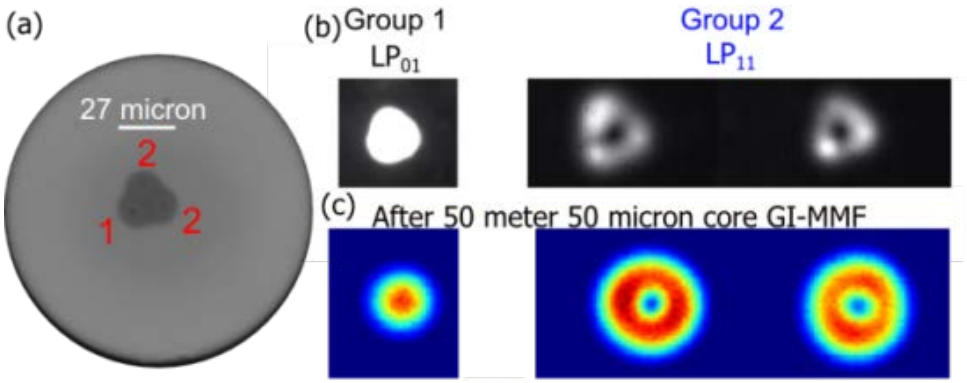

Figure 3.4 (a) End facet of the two mode group selective lantern supporting two mode groups (b) near field intensity profile (c) intensity profiles after 50-m of GI-MMF when illuminated with a C-band broadband source

The time-domain transfer matrix for the three mode group MGS-PL is shown in Figure 3.6 and contains 36 cells. The transfer matrix for a two MGS-PL would contain only 9 cells and is shown as a subset of the three MGS-PL transfer matrix. The columns correspond to the received ports, and the rows to the launched ports. The 50-m GI-MMF contains 8 degenerate mode groups and each group has a unique group delay. Therefore, the time-domain impulse responses can have 8 mode-peaks. The first 3 peaks correspond to group 1, group 2, and group 3 and the last 5 peaks correspond to higher-order-mode (HOM) groups. For a MGS-PL with high mode selectivity, light launched into the fibers in mode group I (I=1,2,3) should be received on the fibers for mode group I. In addition, the majority of the power should be contained in the mode-peak mode groups DGD. These 'signal' cells are on the diagonal and form a 1×1 block for the first group (gray cell), a 2×2 block for the second group (blue cells), and a 3×3 block for the third group (green cells). The energy that does not couple into these cells are crosstalk (red cells). Additionally, the mode peaks indicate which modes are causing crosstalk.

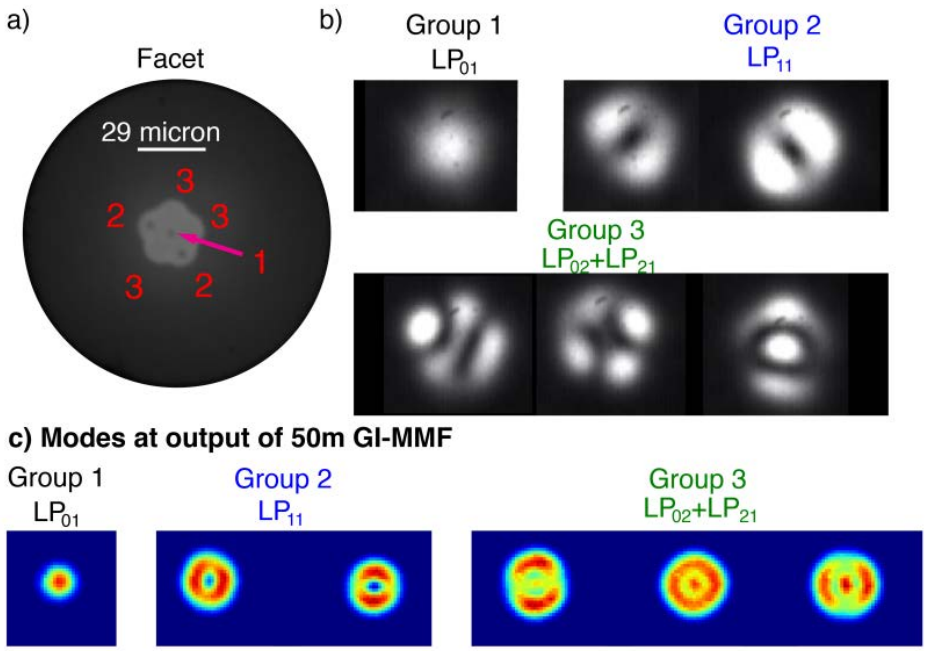

Figure 3.5 (a) end facet of the three mode group selective lantern supporting two mode groups (b) near field intensity profile (c) intensity profiles after 50-m of GI-MMF when illuminated with a C-band broadband source

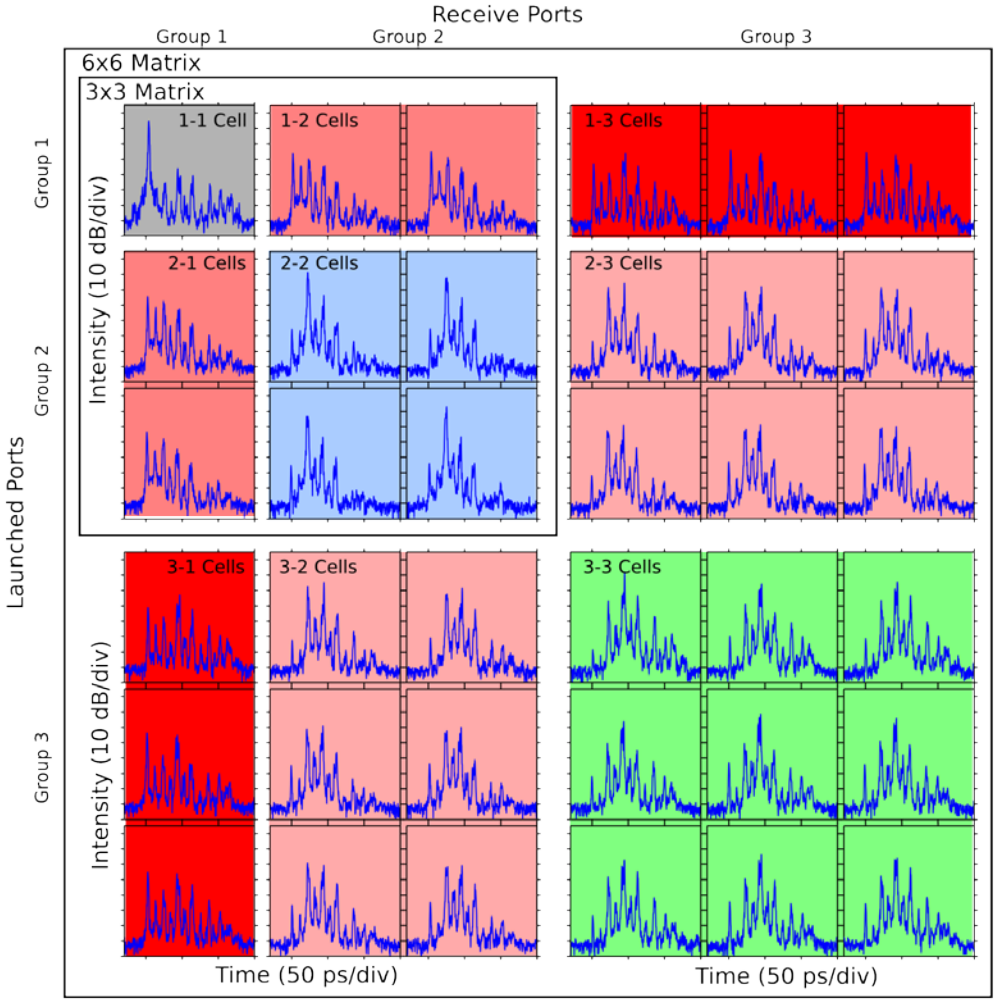

Figure 3.6 Full transfer matrix for the three mode-group MGS-PL (6 spatial modes). Crosstalk between groups are indicated by red cells. Cell blocks on the diagonal are the signal cells. The two mode group MGS-PL matrix is a subset of the 6×6 matrix.

The MGS-PL supporting two mode groups has a transfer matrix that contains 9 elements. The full transfer matrix is not shown, but it would be similar to the 3x3 matrix in Figure 3.6. To quantify mode selectivity we can find the total signal power received in mode group I by summing the 'signal' cells together. The total crosstalk on group I is the summation of the crosstalk cells in the columns corresponding to mode group I. The mode-selectivity for mode group I is defined as the ratio of the crosstalk on group I to the signal power received in mode group I. Figure 3.7 shows

these summations. The 1-1 cell shows the clean excitation of the LP_{01}LP$_{01}$ mode with suppression of the HOMs (e.g., the additional mode peaks). The 2-2 summation (e.g., blue cells in Figure 3.6) shows excitation of the LP_{11} modes with 40-dB rejection of the LP_{01}LP$_{01}$ mode, and about 18-dB rejection of the LP_{02} + LP_{21} modes. The 1-2 summation (1-2 cells in Figure 3.7) shows the total crosstalk between groups, and is roughly 18-dB smaller than the signals. These measurements show that MGS-PL supporting two mode groups has 20-dB mode selectivity for mode group 1 and 2 into the GI-MMF.

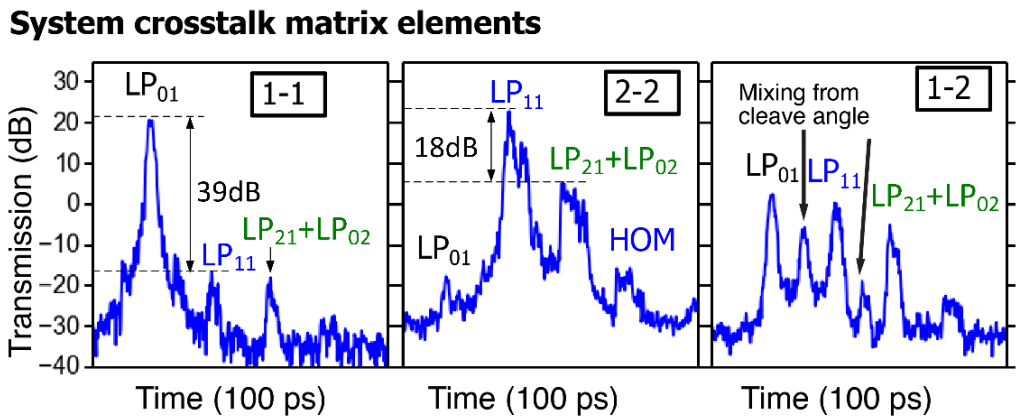

Figure 3.7 Summation of signal and crosstalk cells from the reflection transfer matrix for mode group selective lantern supporting two mode groups.

Next, we analyze the MGS-PL supporting three groups. Figure 3.8 shows the signal cells and the crosstalk cells. The 1-1 cell shows excitation of only the LP_{01}LP$_{01}$ with 31-dB suppression of the mode group LP_{21} + LP_{02} which has the largest crosstalk among all the undesired modes. The 2-2 cell shows excitation of the LP_{11}LP$_{11}$ modes with 40-dB rejection of the LP_{01}LP$_{01}$ mode and 16-dB rejection of the LP_{21} + LP_{02}LP$_{21}$ + LP$_{02}$ modes. The 3-3 cell shows excitation of the LP_{21} + LP_{02}LP$_{21}$ + LP$_{02}$ modes with 35-dB rejection of the LP_{01} mode, 13-dB rejection of the HOM

(fourth peak), and 15-dB rejection of the LP_{11} modes. The mode selectivity is 20-dB, 10-dB and 7-dB for groups 1, 2 and 3, respectively.

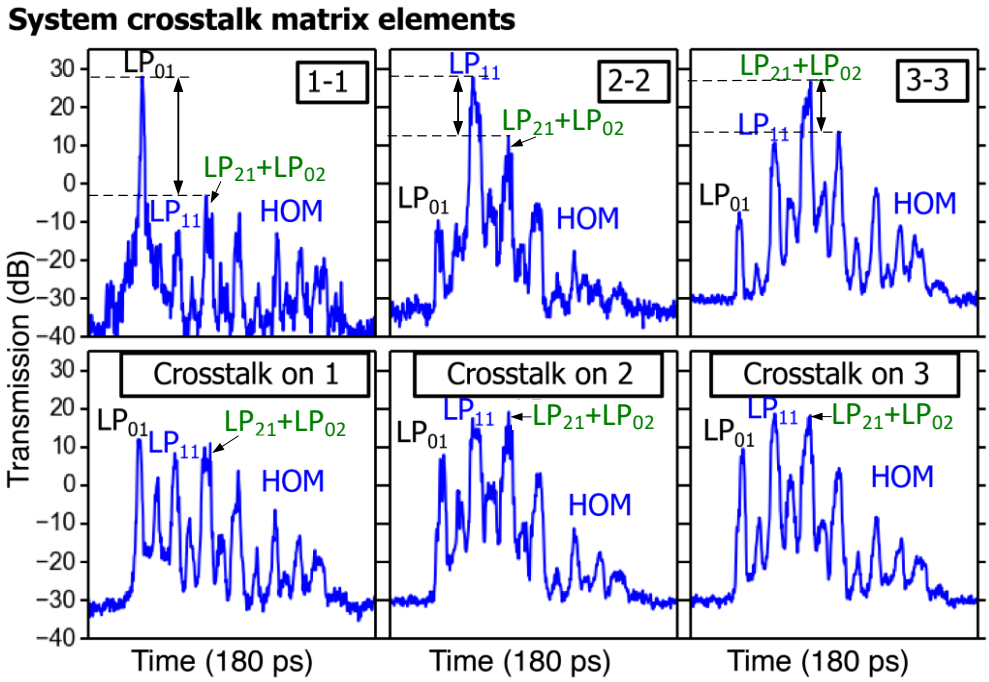

Figure 3.8 Summation of signal and crosstalk cells from reflection transfer matrix for mode group selective lantern supporting three mode groups.

By further optimizing the fabrication processes (fluorine tube size, tapering processing, preparation etc.), the IL of the 6-mode (3-mode group) PL can be below 1 dB when spliced to 6-mode transmission GI fiber. The MDL for a pair of them as Mux and DeMux is around 2 dB across the whole C band.

CHAPTER 4: PHOTONIC LANTERNS SCALING TO MORE MODES USING NOVEL LOW-INDEX DOUBLE CLAD DRILLED MICRO-STRUCTURED PREFORM

For LPs scaling to more modes, in principle, we can keep on with the same method. However, we are encountered with two big obstacles. First, which is from the fabrication point of view, is to maintein the geometry of the photonic lantern input fibers. For 3-mode and 6-mode PL, it is possible to place fibers into right geomtry by hand. But for more modes, it is difficult to achieve it simply by hand. One way to overcome it is to use structures to facilitate fabrication. Both stack and draw preform [51] and drilling preforms [52] can be used for the ease of fabrication. The other obstacle is the adiabaticity requirement. As we have shown in Eq. 3.1 that scaling to N modes requires roughly N^2 times tapering length due to the adiabatic requirement [50]. What is worse is that the new preform adds more cladding material which makes adiabaticity requirement even more difficult to meet.

We demonstrated PLs using double-clad micro-structured preforms fabricated by drilling, which not only ease the fabrication complexity for mode scalablity but also alleviate the adiabatic requirement for lantern tapering. Additionally, the output modes are circular, and the individual cores have less effect on the final mode patterns. For a10-mode (20 vector modes) PL, the IL ranges from 0.6 to 2.0 dB across all the modes when spliced to a 10-mode GI fiber. The MDL for a pair of these PLs reaches a record low level of 4 dB.

4.1. Rationale

Figure 4.1 shows the two double cladding micro-structured drilling preforms for a 10-mode PL, with only slight difference. The proposed double cladding micro-structured preforms is shown in

Fig.1 (b). The material of the inner structure shown in Figure 4.1 (a) is the same as the fiber cladding (refractive index 1.444). The structure we propose is shown in Figure 4.1 (b), whose index (1.442) of the inner cladding (weakly fluorine doped) is lower than the cladding of the input fibers. Hence, this structure is called the low-index double cladding micro-structured preform. In this structure, mode profile evolution is more adiabatic than the structure shown in Figure 4.1(a) for the same tapering length. The reason is the following, as the preform gets tapered down, the fundamental mode launched in each core will become less guided and expand rapidly. Structure in Figure 4.1(a) adds more cladding material, which makes the expansion faster and extend across the entire structure. While for our proposed low-index micro-structured preform, the lower index (1.442 of the inner) which is smaller than the cladding index captures the expanding modes.

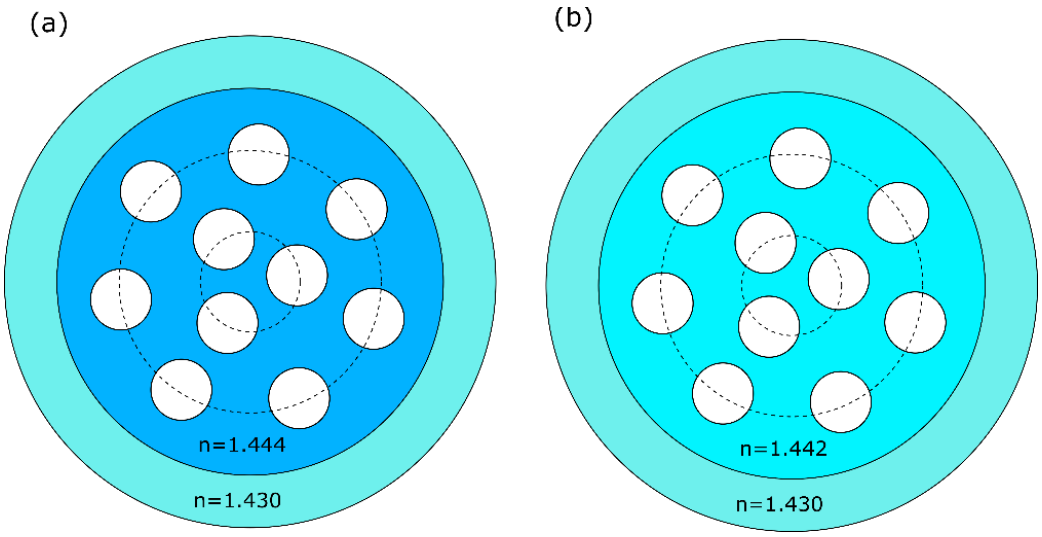

Figure 4.1 Double-clad drilled preform with the refractive index of the inner cladding (a) same as the fiber cladding (b) smaller than fiber cladding

To demonstrate this quantitatively, we simulate mode evolution using the single-core geometries in Figure 4.2(a) and (b). It is the simplified version compared to the structure in Figure 4.1, but the mechanism is similar. For both cases, the input fibers are the same GI-FMF. In Figure

4.2(a), the cladding of the fiber has the same refractive index as the inner cladding of the preform as indicated by the same color, while in Figure 4.2(b), the index of the fiber cladding is higher than that of the inner cladding of the preform as indicated by a lighter color. We then calculate the profiles of the fundamental of the both structures at different tapering ratios. Figure 4.2(c) shows the mode-field diameter (MFD) of the fundamental mode versus the taper ratio (from 1 to 0.03). The MFD of both cases initially decreases at the same rate until the taper ratio around 0.3, after which The MFD starts to increase. However, the slope of the increase of MFD is more than five times for structure (a) than the structure (b).

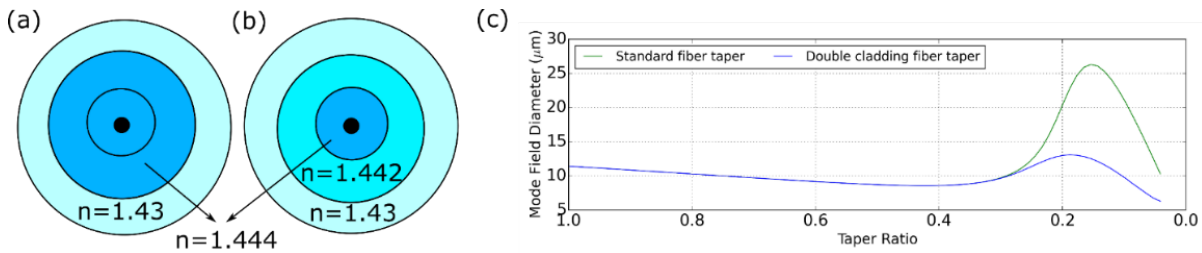

Figure 4.2 Simplified one hole structure of double cladding drilled preform with GI-FMF inserted and the inner cladding of the one hole structure has the refractive index (a) same as the fiber cladding (b) smaller than the fiber cladding (c) mode field diameter vs taper ratio for both cases

4.2. Non-mode selective photonic lantern

PLs can be roughly divided into two categories: mode selective and non-mode selective PL. If the input fibers of the PLs are dissimilar, they become mode selective [46]. One important type of mode selective lantern is mode group selective PLs [53], which are suitable for both long haul transmission system and short reach applications [54–57]. Mode group selective PLs can selectively excite modes belonging to certain mode group. The transfer matrix of mode group selective PL is block diagonal [53] due to mode group selectivity.

For non-mode selective PLs, the input fibers are identical. To make the PL shown in Figure 4.1(b), we use 10 identical GI-FMFs as input fibers. The transfer matrix of a non-mode-selective

PL, in general, cannot be obtained easily, except for a 3-mode non-mode-selective PL. For a 3-mode non-mode-selective PL, the transfer matrix can be derived from symmetry considerations alone. But for larger-size non-mode-selective PLs, such kind of symmetry does not exist. Since the input fibers are identical, the transfer matrix should be dominated by the structure, i.e., the geometrical arrangement of the input fibers and the claddings, of the PL.

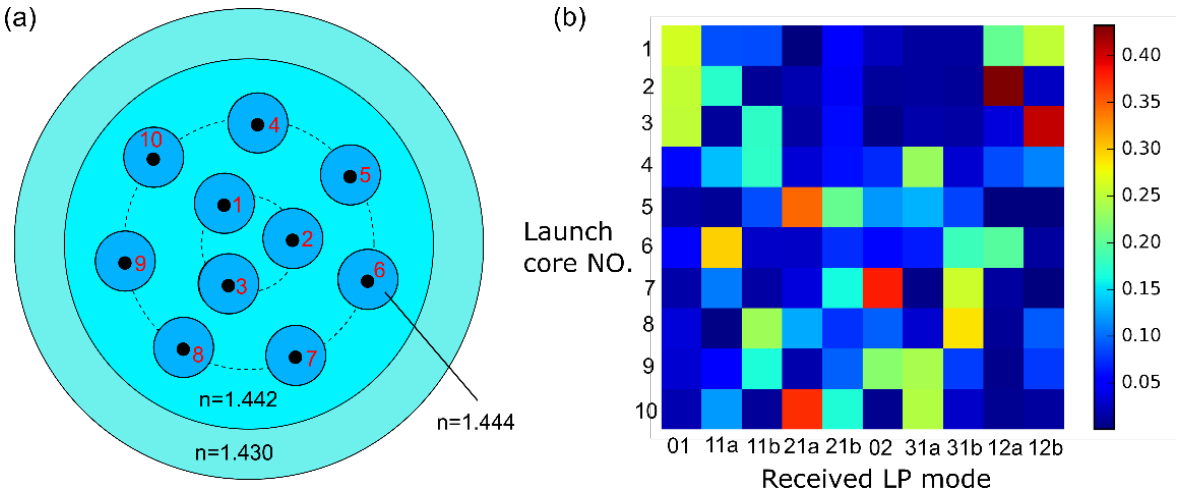

Figure 4.3(a) Double-clad drilled preform with labeled cores (b) Intensity coupling matrix between launched labeled core and received LP mode at the end of the photonic lantern.

Due to the complexity of its transfer matrix, the only way to effectively characterize a non-mode-selective PL is to measure its IL and MDL instead of only measuring the power transfer characteristics of the PL. We used the beam propagation method to first numerically calculate the transfer matrix and verify the effectiveness of the proposed structure, such as shown in Figure 4.3(a), from the MDL and IL. The total length of the photonic lanterns in the simulations is 5 cm and the linear taper ratio is 1/36. We launch fundamental mode into each input fiber one at a time, then collect the output field at the output few-mode fiber of the PL. The transfer matrix can be calculated by computing the overlap integrals between the output field and the 10 lowest-order spatial modes of output few-mode fiber of the PL. MDL and IL can also be derived from the

transfer matrix. The simulated IL and MDL obtained from the simulations are 0.01dB and 0.03dB. Therefore, in theory, nearly lossless 10-mode PLs are possible using the preform shown in Figure 4.3(a) within a taper length of only 5 cm.

4.3. Fabrication

We realized the preform proposed in Figure 4.1(b) in several steps. First, we fabricated the inner cladding and outer cladding individually. The micro-structured inner cladding, shown in Figure 4.4 (a), was fabricated from a light fluorine-doped rod by drilling. The outer cladding shown in Figure 4.4 (b) is a heavily fluorine-doped tube. The inner and outer cladding have refractive indices of 1.442 and 1.43, respectively. Ten holes with a diameter of 130 μm arranged in two circles were drilled into the inner cladding. The small circle of diameter 203 μm has three holes while the larger circle of diameter 528 μm has seven holes. The outer diameter of the inner cladding is 780 μm. Ten identical GI FMFs were inserted into the 10 holes. The heavily-doped outer cladding has an inner diameter around 350 μm and thickness of 280 μm. Since the inner diameter of outer cladding is smaller than the outer diameter of inner cladding, we tapered the inner cladding by a ratio of 1/2.4. At this taper ratio, the fundamental mode in the input GI FMF is still well confined in the core. Then the inner cladding was inserted into the outer cladding to complete the preform for the PL. Lastly, the entire preform was tapered by a ratio of 1/16 as shown in Figure 4.4 (c). The photonic lantern was then cleaved and spliced to a piece of short 10-mode GI fiber.

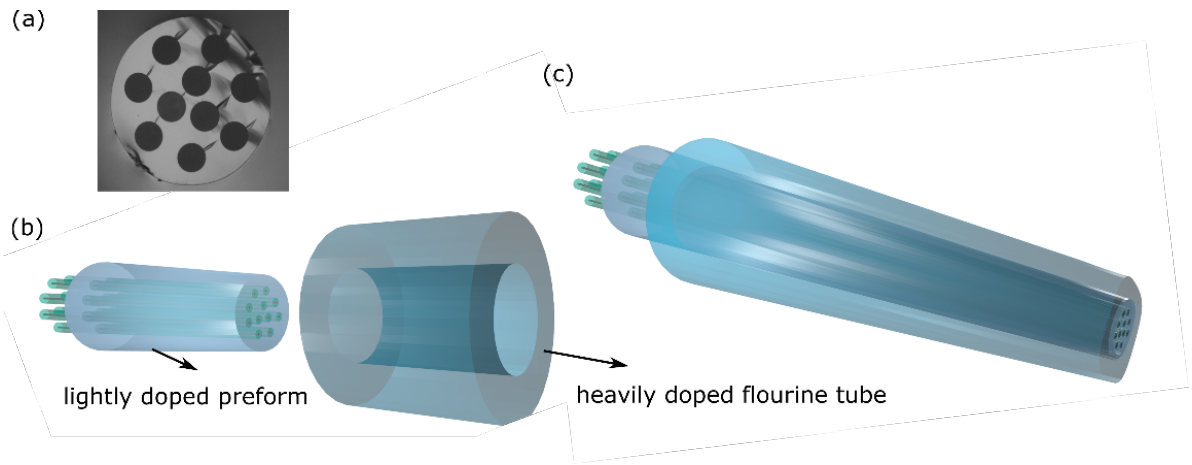

Figure 4.4 (a) The facet image of the drilled preform as the inner cladding of the proposed preform (b) insert the tapered lightly doped preform into heavily doped fluorine tube to form the proposed structure (c) final taper for the fabrication of the photonic lantern.

4.4. Characterization

The output intensity profiles of the PL before and after splicing to 10-mode GI-FMF are shown in Figure 4.5 and Figure 4.6. From the Figure 4.5, we can see that the output intensity of each core launch is truly non mode selective. However, we can still observe that the inner three cores couples largely to LP_{01} and LP_{11}. The quality of the PL must be evaluated by both IL and MDL after spliced to the 10m 10-mode GI-FMF.

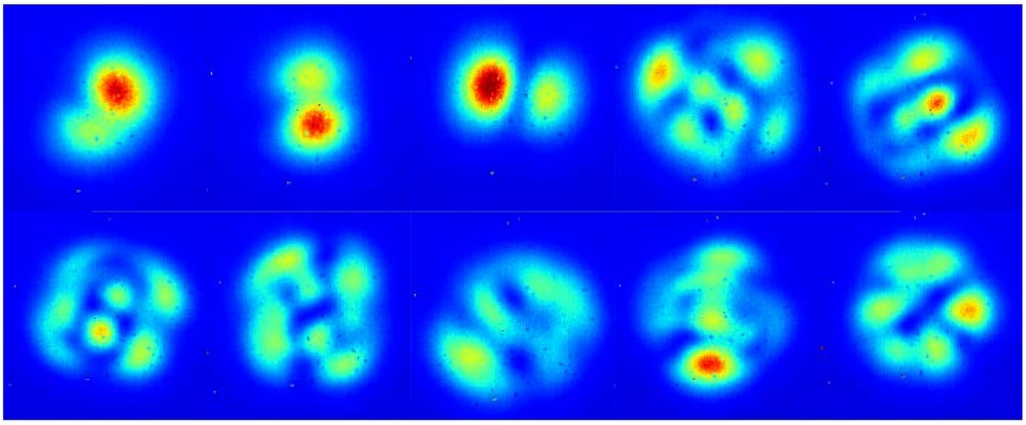

Figure 4.5 Mode intensity profile of photonic lantern before splicing to the 10 mode GI fiber.

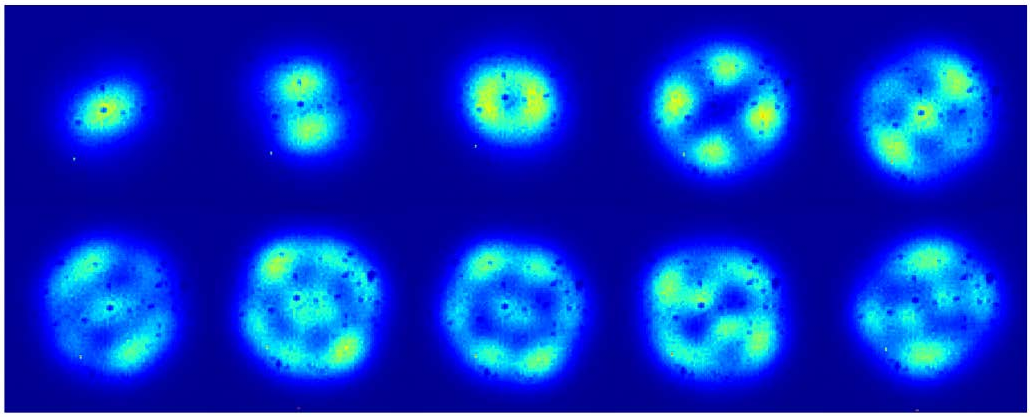

Figure 4.6 Mode intensity profile of photonic lantern after spliceing to the 10 mode GI fiber.

The loss for the ten input fibers range from 0.6 dB to 2 dB and the IL is less than 1.5 dB. MDL measurements require measurement of the full amplitude and phase transfer matrix. Since we made only one device, the MDL is measured in reflection mode. The setup for the characterization of MDL is shown in Figure 4.7 which includes a swept-wavelength interferometer (SWI) and the 10-mode PL under test. The SWI comprises a tunable laser source, a polarization Mux, a fiber interferometer and a polarization-diversity coherent receiver. The receiver includes one polarization beam splitter (PBS), two 2 x 2 couplers, two balanced photodiodes and two 100-MS/s analog-to-digital converters. In the experiment, light coming from the swept-wavelength laser source is split into two branches, the signal and the reference. In the signal branch, a polarization multiplexer ensures that two orthogonal polarizations are launched with same power. Fiber delays were added at the input and output of the signal to differentiate the input-output response in the time domain. The swept-wavelength signal goes through one fiber delay bank into the PL and gets reflected by a mirror. Then it goes through the PL from the opposite side, enters the other delay bank and finally into the receiver. In this arrangement, light goes through the photonic lantern back and forth, yielding characterization of a pair of identical PLs. The full 20×20 (20 vector modes)

complex transfer matrix at each wavelength can be obtained as shown in [58,59]. The MDL can be calculated by using singular value decomposition (SVD) of the transfer matrix at each wavelength. The MDL for the pair of identical PLs over the entire C band (191.45 – 195.85 THz) is around 4 dB, as shown in Figure 4.8.The variation of MDL comes from noise and can be cleaned up by averaging over more traces.

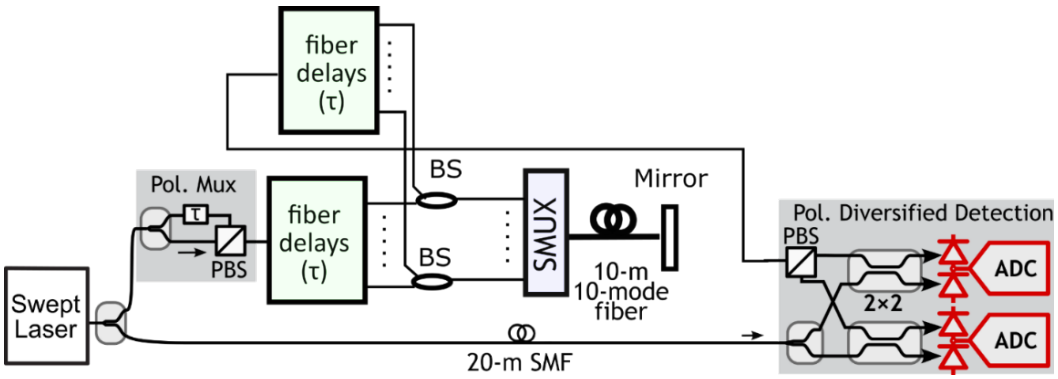

Figure 4.7 Experimental setup for transfer matrix measurement.

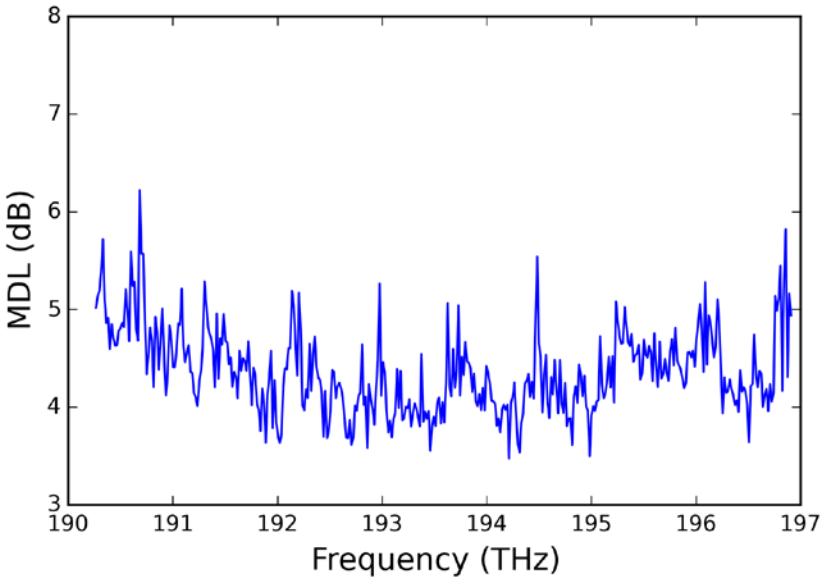

Figure 4.8 MDL vs frequency

CHAPTER 5: SPACE DIVISION MULTIPLEXING AMPLIFIERS

SDM amplifiers are indispensable components for transmission systems [60–66]. We need few-mode amplifier for FMF transmission and multi-core amplifier for MCF transmission. Amplification using SDM amplifiers adds further equal MDG requirement. Perfect amplification requires all the spatial modes to have the same gain characteristics.

For multi-core amplifier, the requirement is to have the same gain in each core, which requires that the signals from MCF be launched into the amplifier with negligible loss and the pump light be launched into the amplifier channel with equal power. Two pump scheme can be used for amplification, core pump and cladding pump. For core pump scheme, we have two options, fiber based and free space. The fiber based method requires two fan-in fan-out couplers [67–69] for both signal and pump light to go into the amplifier. The first fan-in fan-out coupler convert the N spatial channels of MCFs into N fundamental modes of SMFs, the pump and the signal are then combined by WDM. Then through the second fan-in fan-out coupler, N fundamental modes of SMFs with pump light are coupled to N spatial channels of MCFs. This technique does not require very complex components and is in general cheap. However, at current stage, the IL and MDL of the fan-in fan-out are still not negligible and the loss increases with the core number. The other method for core pump is free space, this method requires bulk free space optical component. However, the loss can be made to be very low. The other pump scheme cladding pump [70–74]. Pump light is launched into the cladding modes of the MCF through side pump. The non-zero intensity overlap between the cladding modes and core mode ensures the amplification. This technique ensures very compact structure, MCF can be directly connected to the multi-core amplifier with pump fiber fused to the multi-core amplifier. Also this structure has very low IL and MDL.

However, one drawback is this scheme requires large amount of pump power, which is not energy efficient.

The pump scheme for few-mode amplifier is quite similar. For core pump, we can use free space pump scheme and directional coupler based core pump. Free space pump scheme combines the signal and pump in free space while the directional coupler which couples the single mode pump of 980nm into the FMF core mode. The cladding pump scheme is the same as multi-core amplifiers. MDG in few-mode amplifiers is slightly more complicated than MCF since the gain is related to the pump intensity distribution, erbium dopant distribution and the signal mode intensity distribution. Thus MDG depends on the pump mode, erbium dopant distribution. Methods to achieve low MDG have been widely explored by tailoring the erbium dopant distribution [75] and controlling the pump modes [76].

In the following chapters, we first discuss our method for achieving low MDG of few-mode amplifier. Then we discuss a novel way of measuring MDG of few-mode amplifier using mode selective PL. After that, we discuss the application in turbulence resisted free space optical (FSO) communication.

5.1. Multi-mode amplifier for the amplification of few mode fiber channels

We present a much simpler scheme to minimize the MDG that is compatible with cladding pump by intentionally oversizing the core to support many more modes required. This ensures that the desired amplified modes are well confined inside the core to maximize each modes overlap with the gain, and the cladding pump ensures that the gain medium is illuminated uniformly. Despite of the fact many more modes are supported, the performance is not degraded because mode mixing is negligible in the short amplifying fiber. We demonstrate amplification of 10 spatial modes with MDG below 2 dB and output power of 25 dBm.

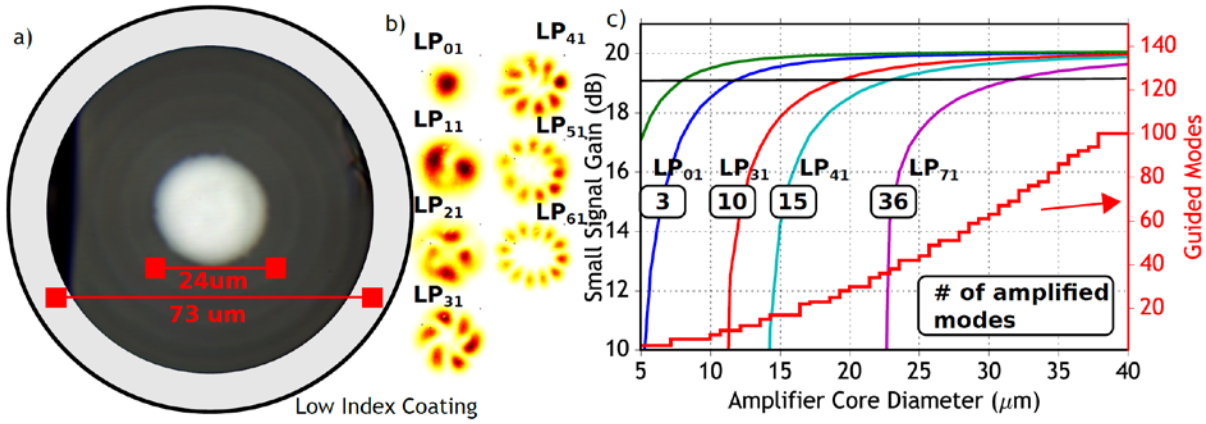

Figure 5.1 a) Er-doped fiber facet image. b) modes from each mode group. c) mode dependent small signal gain vs. amplifier core diameter for different mode groups. The refractive index step is 2.3×10^{3}.

The amplifier is designed to minimize both MDG for up to 15-spatial modes and MDL when spliced to the transmission fiber which is typically graded-index to minimize the differential group delay. Figure 5.1(a) shows the facet image of erbium doped fiber (EDF). The core has a diameter of 22-24 μm, a refractive index (RI) difference of 2.3×10^{-3} with respect to the cladding and supports approximately 26-28 spatial modes. Figure 5.1 (b) shows measured mode profiles at the output of a 20m EDF for mode groups 1 through 7. To guide multi-mode pump light in the cladding, the polymer coating has a numerical aperture (NA) of 0.46 with respect to the glass cladding. The cladding diameter is restricted to 73 μm to enhance the pump intensity. The erbium ion concentration is $4.5 \times 10^{25} m^{-3}$ and can provide a maximum gain around 10dB/m at 1550 nm.

Figure 5.1(c) shows a simulation of the small signal MDG for different modes in a uniform doped core for a target LP_{01} gain of 20 dB assuming uniform illumination of the gain material using cladding pump. It is calculated as $\exp(2gL\Gamma_{ij})$ where Γ_{ij} is the intensity overlap integral of mode LP_{ij} with the core and gL (gain × length) is a scaling factor to adjust the LP_{01} gain to 20 dB.

When the gain is above 19 dB for the amplified mode, the MDG is less than 1 dB. 1 dB MDG is achieved for 10(15) modes with the amplifying core supporting 20(28) modes, respectively.

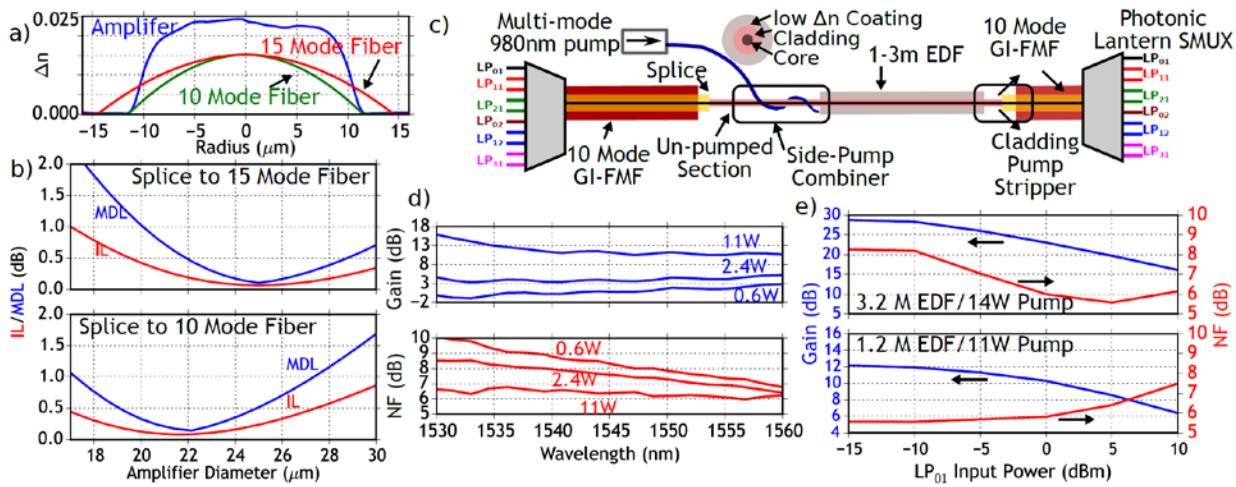

Figure 5.2 a) Measured refractive index profiles. b) Simulated splice loss between amplifier and transmission fiber. c) Amplifier characterization. d) Gain and noise figure for 1.2-m EDF under different coupled pump powers. e) Gain and noise figure at 1550 nm vs. signal input power.

Any improvements by minimizing the MDG are undone if it is difficult to eliminate MDL at the splice to the GI transmission fiber. Figure 5.2 (a) shows the refractive index cross section of the amplifier and a 10 and 15 mode transmission fiber. Figure 5.2 (b) shows the simulated MDL and IL for splices to a 10 and 15 mode GI fiber indicating that an amplifying core of 24 μm will have splice induced IL and MDL well below 1 dB.

The amplifier NF, gain and the saturated output power are characterized by launching and receiving the LP_{01} mode. Figure 5.2 (c) shows the setup for testing the amplifier. Mode selective PLs spliced to a 5 m piece of 10 mode GI fiber are used at the input and output to couple SMFs to all the modes of the amplifier. Side pump is used to couple the multi-mode pump light into the cladding modes (60% efficient) and eliminates the need for any wavelength dependent components.

Figure 5.2 (d) shows the gain and NF for a 1.2 m EDF under different pump powers. Approximately 11 W of 980 nm pump power can fully invert the gain which is indicated by the large gain at 1530 nm and flat external NF of 6 dB. Figure 5.2 (e) shows the gain and NF under different signal powers at 1550 nm for a 1.2 m and 3.2 m EDF. The 3.2 m EDF can achieve over 25 dBm output power with input power between 5 and 10 dBm, however its NF performance suffers due to self-saturation of the input from backwards amplified spontaneous emission (ASE) which improves slightly as the input signal power is increased. From these results, the optimal EDF length for a transmission amplifier 20 dB gain and low NF is around 2 m.

In a fiber without mode mixing, MDG can be measured by launching and receiving each mode one by one. However, in real fibers the modes mix and scramble in the fibers and at splice points making mode selective excitation and reception erroneous. In particular, in this setup, the mode selectivity is limited by the mode Mux, strong intra mode group mixing in the 10 mode GI fiber, and at the 4 splices between the mode Mux, 10 mode fiber and the amplifier to less than 5 dB. Therefore, the most accurate way to measure MDL/MDG is to characterize the amplitude and phase transfer matrix of the amplifier between each input and output pair across all wavelengths. From this transfer matrix, the MDL/MDG and IL can be computed by an eigen-analysis of the transfer matrix.

We measure the TM using a SWI with spatial diversity. Figure 5.3(a) shows the intensity of the 20×20 transfer matrix (10 spatial modes and 2 polarizations each) measured across the entire C band. The matrix is dense which indicates some mode scrambling from the inputs to the outputs. Each one of the cells contains the full amplitude and phase information across the entire measurement range. Figure 5.3 (b) shows the impulse response computed by taking the Fourier transform of the impulse response of a single cell. The first 4 mode groups are 25 dB stronger than

the unused mode groups 5, 6 and 7 indicating good suppression of the additional unused spatial modes.

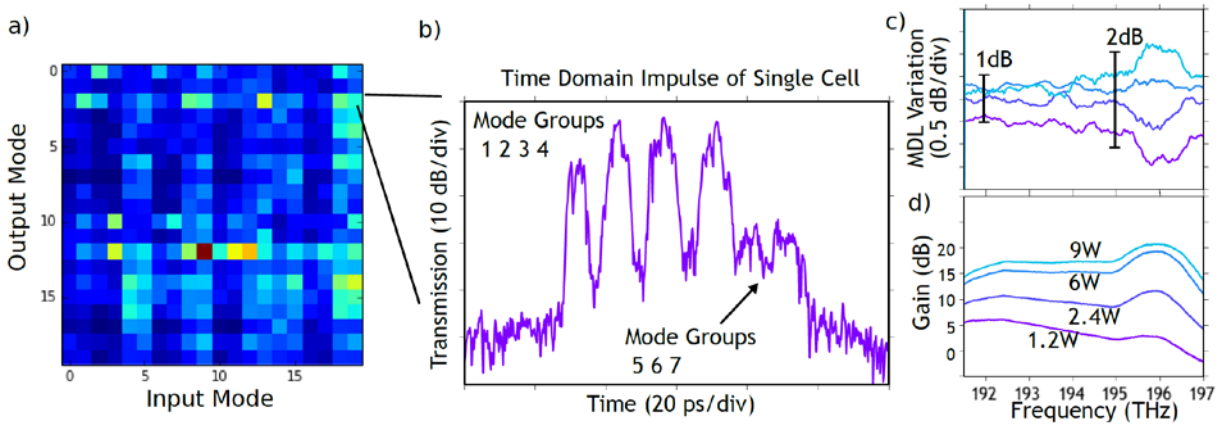

Figure 5.3 Mode-dependent gain measurements for 10 spatial modes of a 1.6-m EDF. a) Transfer matrix, b) impulse response, c) mode dependent loss/gain, and mode averaged gain.

Figure 5.3 (c) shows the MDG change as the coupled pump power varies from 1.2W to 9W. The background MDL is around 8.5 dB and is from the MDG inside the two PL. The important point is the MDG changes less than 2 dB as the pump power is varied. This means that all modes experience the same gain regardless of the inversion of the gain material.

5.2. Spatially and spectrally gain characterization of few mode amplifier using photonic lantern

As already mentioned, achieving optimal performance for long-haul transmission systems requires that FMF amplifiers produce wide band gain across the entire C-band with negligible mode-dependent gain, and with a low noise figure (NF). These properties are a function of pump power, input signal power, and EDF length given Erbium distribution and concentration. Therefore, it is critical to characterize the gain of the few mode EDFAs based on input signal and pump conditions as a function of amplifier length. Standard techniques such as cut-back method can determine the gain vs. length, but they are time-consuming, destructive and not applicable for the measurement

of backward or bi-directionally pumped amplifiers. Alternatively, measuring the time-resolved Rayleigh backscattering [77] using a swept wavelength interferometer (SWI) operated in the reflection mode is non-destructive and has been demonstrated to determine the distributed gain and appropriate length for SMF amplifiers with resolution as short as 2 cm [78,79]. We further develop the SWI technique to characterize few mode EDFAs by measuring the time-resolved backscattered light for spatial channels. We measured the spatially and spectrally resolved gain across the C band of a few mode EDFA supporting 3 spatial modes. To verify the validity of SWI, we compared the results to well established cut-back measurements.

Figure 5.4 shows the schematic of the SWI used for the characterization of the SDM EDFA [80]. SWI capable of characterizing single mode EDFA is well established in papers [80,81]. We will provide a brief description of operation principles and discuss spatially and spectrally modal gain measurement for few mode EDFA.

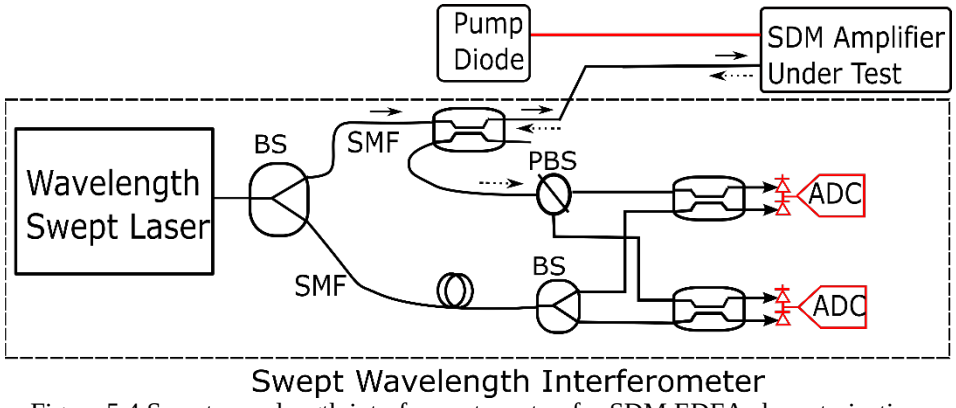

Figure 5.4 Swept wavelength interferometer setup for SDM EDFA characterization.

A SWI comprises of a tunable laser source, a fiber interferometer, and a polarization diversified coherent receiver. The receiver includes one polarization beam splitter (PBS), two 2×2 couplers, two balanced photodiodes and two 100-MS/s analog-to-digital converters. Laser light coming from the wavelength swept laser is split into two arms of the interferometer: signal and

reference. The signal light is coupled into one input of the 2×2 coupler and the Rayleigh backscattered light from the SDM amplifier couples out of the coupler from the other input port. Then, the Rayleigh backscattered light from the SDM amplifier beats with the reference beam in the polarization diversity receiver which produces an interferogram that contains the amplitude and phase information of the backscatter vs. frequency. To further explain this, we consider one polarization for simplicity. An ideal swept laser source's electric field is expressed as:

$$E_L(t) = E_0 \exp[i2\pi(\upsilon_0 t + \gamma t^2 / 2)] \tag{6.1}$$

Where $E_L(t)$ is the electric field of the local oscillator, E_0 is the amplitude, γ is the swept rate of the tunable laser. The instantaneous frequency $v(t)$ is the derivative of the phase in (4.1):

$$\upsilon(t) = \upsilon_0 + \gamma t \tag{6.2}$$

The backward reflected signal $E_{\mathrm{sig}}(t)$ can be represented as:

$$E_{sig}(t) = \int h(\tau) E_0 \cdot \exp\{i2\pi[\upsilon_0(t-\tau) + \gamma(t-\tau)^2 / 2]\} d\tau \tag{6.3}$$

Where τ is the delay between the signal and the reference, h is the impulse response of the device under test (DUT). The beat current $i_{\mathrm{sig}}(t)$ at the receiver can be expressed as:

$$i_{sig}(t) = C_1 \cdot \mathrm{Re}(E_L(t) E_{sig}{}^*(t)) \tag{6.4}$$

Where C_1 is a constant. Inserting (6.1) and (6.3) into (6.4), we can derive:

$$i_{sig}(t) = C_1 \cdot \mathrm{Re}\{(\int E_0{}^* E_0 h(\tau) \exp[i2\pi(\upsilon_0 \tau - \gamma \tau^2 / 2 + \gamma t \tau)] d\tau\} \tag{6.5}$$

Equivalently, we can write the beat current as the instantaneous frequency through the relation (6.2):

$$i_{sig}(\upsilon) = C_1 \cdot \mathrm{Re}\{(\int E_0{}^* E_0 h(\tau) \exp[-i2\pi\gamma\tau^2 / 2] \exp[i2\pi\upsilon\tau] d\tau\} \tag{4.6}$$

Equation (6.5) describes the signal output at the receiver which gives an interferogram that contains the amplitude and phase of the backscatter vs frequency. It can also be viewed as the Fourier transform of the kernel $h(\tau)\exp(-i\gamma\tau^2)$ once $i_{sig}(t)$ is normalized to $E_0^* E_0 C_1$. The phase and amplitude of the kernel can be recovered from the real part of $i_{sig}(v)$ through a Hilbert transform of $i_{sig}(t)$ provided that the $h(\tau)$ is single sided. The squared absolute value of the recovered kernel gives the intensity impulse respose $I_{sig}(t)$ in time domain, which can also be written as $I_{sig}(L)$ through the relation:

$$L = v_g t / 2 \tag{6.7}$$

$I_{sig}(L)$ is proportional to the backward reflected signal power averaged across the swept bandwidth. Also for the amplifier, the unwanted backward amplified spontaneous emission (ASE) and back reflected forward ASE also needs to be taken into account at the receiver. The total ASE noise contribution at the receiver is $i_{ASE}(\nu)$. Since $i_{ASE}(\nu)$ is incoherent with the laser, only the ASE that beats with E_{LO} and falls within the detector bandwidth is added to the measurement. The complete measured current at the receiver is:

$$i(\upsilon) = i_{sig}(\upsilon) + i_{ASE}(\upsilon) \tag{6.8}$$

In the spectral domain, $i_{ASE}(\nu)$ shows the accumulated ASE noise beat with reference beam averaged through the amplifier length. In the time domain impulse response, $I_{ASE}(t)$ spreads across the entire time domain and produces a power offset to the trace. The measured impulse response $I(L)$ (in dB) is the sum of signal impulse response $I_{sig}(L)$ and ASE contribution $I_{ASE}(L)$. Since $I_{ASE}(L)$ simply produces a power offset, the gain $G(L_0)$ averaged across the swept bandwidth at amplifier length $L=L_0$ can be deduced directly from the measured current $I(L)$:

$$G(L_0) = (I(L_0) - I(L=0)) / 2 \tag{6.9}$$

Spatially and spectrally resolved modal gain can be estimated by further exploiting the data. Spectral gain at amplifier length $L=L_0$ can be estimated by:

$$G(L_0,\upsilon) = (i_{sig}(L_0,\upsilon) - i_{sig}(L=0,\upsilon))/2 \tag{6.10}$$

Where $i_{\mathrm{sig}}(L_0,\upsilon)$ is the current representing spectrally backward reflected signal power at amplifier length $L=L_0$ and $i_{\mathrm{sig}}(L=0,\upsilon)$ is the current representing spectrally backward reflected power at the beginning of the amplifier. $i_{\mathrm{sig}}(L=0,\upsilon)$ only reflects Rayleigh backscattering level of the amplifier and can be approximated as a constant. Thus $i_{\mathrm{sig}}(L=0,\upsilon)$ can be written as $i_{\mathrm{sig}}(L=0)$. $i_{\mathrm{sig}}(L=0)$ can be estimated when no pump or small pump is launched into the amplifier. $i_{\mathrm{sig}}(L_0,\upsilon)$ can be calculated by:

$$i_{sig}(L_0,\upsilon) = i_{tot}(L_0,\upsilon) - i_{ASE}(\upsilon) \tag{6.11}$$

Where $i_{tot}(L_0,\upsilon)$ is the current representing spectrally backward reflected measured power at amplifier length $L=L_0$. $I(L_0,\upsilon)$ can be calculated by retrieving a block of data points of $I(L)$ centered at $L=L_0$, multiplying by a Hanning window to prevent spectral leakage and then performing a Fourier transform. $I(L)$ is the intensity impulse response calculated from the Hilbert transform of the measured current at the receiver $i(\upsilon)$. $i_{\mathrm{ASE}}(\upsilon)$ can be measured at the location before or after the amplifier where only ASE dominates.

Characterization of few-mode fiber amplifiers need to selectively excite and receive spatial modes. For the SWI technique, one additional high extinction ratio fiber based mode multiplexer is required. Fiber based mode multiplexers can be used to excite one spatial mode at the input of the few mode fiber amplifier and collect the backscattered light of the same spatial mode. Some high-performance fiber multiplexers are mode selective photonic lanterns [53] and directional coupler pairs [48]. In this experiment, mode selective photonic lantern was used.

The 3 spatial mode selective photonic lantern was first spliced to a 3-mode GIF. The losses for LP_{01} and LP_{11} mode are 0.4 dB and 1.8dB at 1550nm and the extinction ratio is better than 12 dB at the lantern output. The GIF was then spliced to the few mode EDF which has step-index profile. Figure 5.5 (a) shows the geometry structure of the few mode EDF. The core diameter and NA of the EDF are 15 μm and 0.1 respectively. Figure 5.5(b) shows the mode intensity profile from the few mode EDF at wavelength 980nm (above) and 1550nm (below). To estimate the loss of the splice induced by mode mismatch, the photonic lantern was first spliced to a passive fiber which has the same index profile as the EDF. The loss measured for LP_{01} is 0.6dB and the loss for LP_{11} is around 1.4- 1.7dB. The total loss difference is compensated at the swept laser.

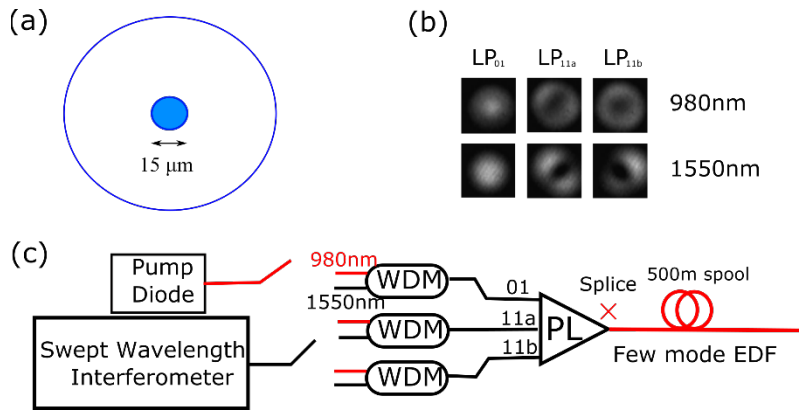

Figure 5.5 (a) Geometry of few mode fiber amplifier (b) mode intensity profile at 980nm and 1550nm when spliced to the few mode EDF (c) experimental setup for the characterization of few mode amplifier.

Figure 5.5 (c) shows the experimental setup for characterizing few mode amplifier. The pump light is coupled into the few mode EDF through WDM and photonic lantern. The pump mode can be either LP_{01}, LP_{11} or mixed. In this experiment, we launched and measured the gain one spatial mode with LP_{01} pump. For the amplifier fully loaded with spatial modes, this technique is still available given calculated or characterized Rayleigh backward coupling matrix. The signal power at the lantern input for LP_{01} and one of LP_{11} (either LP_{11a} or LP_{11b} would have similar amplification behavior) characterization are -11.5dBm and -9dBm so that the signal power levels fed into the

EDF are the same for both modes. The 2.5 dB input power difference comes from the loss difference of two spatial modes from the photonic lantern to the EDF. The same amount of input power fed into the EDF allows the comparison of mode dependent gains between two modes. The EDF length in the experiment is 500 m, which eliminates the need of coreless fiber since light would be totally absorbed and attenuated at the end facet of the EDF.

By SWI technique, we can estimate spatially and spectrally resolved modal gain and also calculate the single trip gain slope of LP_{01} and LP_{11}. The round trip gain averaged across C band and spectrally resolved gain at $L = 14\ m$ of LP_{01} are shown in Figure 5.6 (a) and (b). In Figure 5.7(a) and (b), the round trip gain and spectrally resolved gain at $L = 14\ m$ of LP_{11} are illustrated. From Figure 5.6(a) and Figure 5.7(a), in the linear region, the single trip gain slopes for LP_{01} and LP_{11} are approximately 2.5 dB/m and 2 dB/m. The spectrally resolved modal gains of LP_{01} and LP_{11} at $L = 14\ m$ are shown in Figure 5.6 (b) and Figure 5.7(b). The signal gain spectrum is flat for LP_{01} while tilted towards longer wavelength for LP_{11}. The modal dependent gain varies from 3dB to 5dB across the C band.

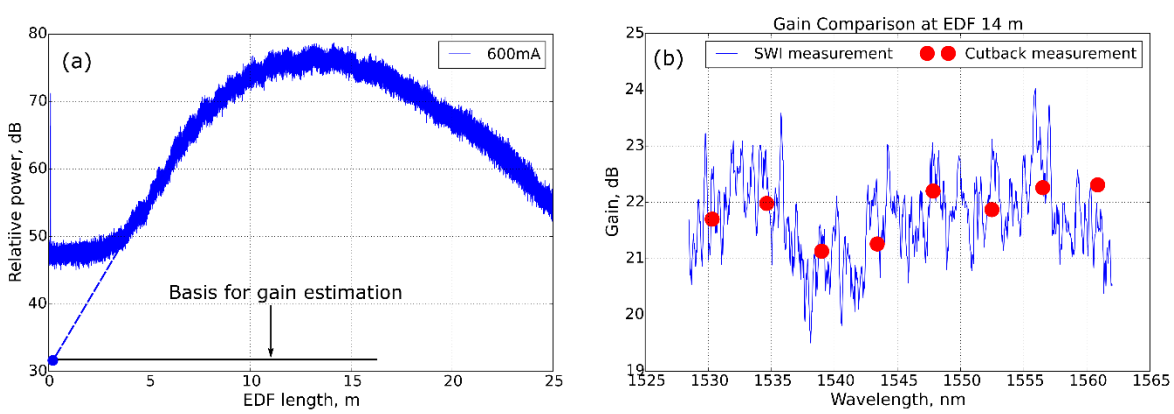

Figure 5.6 (a) The round trip gain of LP_{01} (b) the comparison between SWI measurement and cutback measurement at EDF length 14 m.

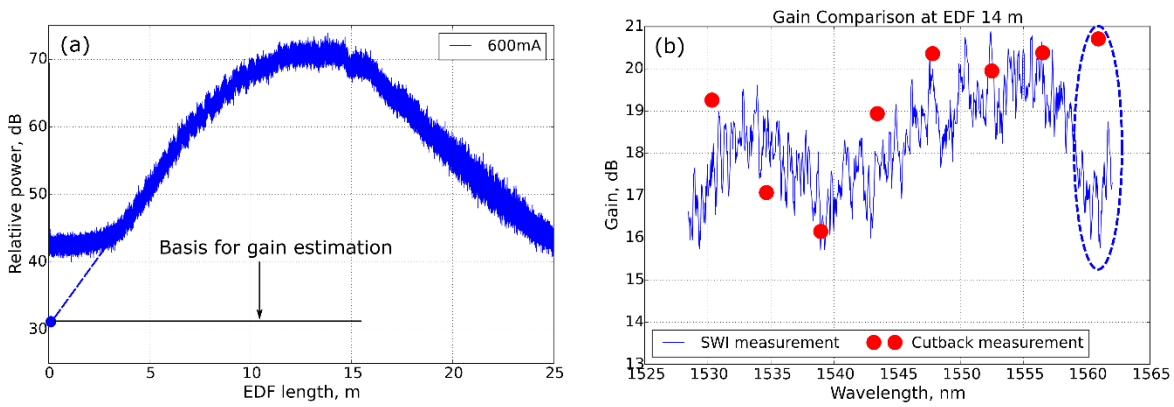

Figure 5.7 (a) The round trip gain of LP_{11} (b) the comparison between SWI measurement and cutback measurement at EDF length 14 m.

The cut back methods were performed at $L = 14\,m$ as comparison. For LP_{01}, the two measurements agree well as shown in Figure 5.6 (b). For LP_{11}, two measurements agree well within 1 dB except for the wavelength around 1560nm as shown in Figure 5.7 (b). That distinct point is due to the mode beating between LP_{01} and LP_{11}, it comes from the crosstalk of photonic lantern and may come more from the splice between the EDF and the GIF due to fiber mode mismatch and splice offset. The possible reason why interference is first observed at longer wavelength is that the modal delay of the EDF between LP_{01} and LP_{11} is larger at longer wavelength, which makes beating between LP_{01} and LP_{11} faster.

By using intermediate fiber with better modal match to the EDF or optimizing the photonic lantern with better mode extinction ratio, the modal crosstalk can be significantly suppressed and the accuracy of the proposed SWI solution can be improved.

5.3. Turbulence-resistant free-space optical communication using few-mode preamplified receiver

The low MDG amplifier mentioned can find another niche application in turbulence-resistant FSO communications. FSO communication offers an orders-of-magnitude increase in transmission capacity, while simultaneously reducing antenna size compared to that of modern radio-frequency (RF) technology. Unfortunately, atmospheric turbulence distorts the wavefront, resulting in both amplitude and phase errors at the detector [82]. Several methods to combat turbulence for FSO have been investigated including arrayed incoherent receivers [83], pulse-position modulation signaling with coherent arrayed receivers [84], and digital coherent arrays with electronic wavefront correction [85]. Nevertheless, the state of the art in FSO communication is dominated by the use of adaptive optics (AO) to correct for wavefront distortions caused by atmospheric turbulence, followed by optically single-mode preamplified receivers. If wavefront correction is perfect, such a system can restore the ideal receiver sensitivity at 38.3 photons/bit for OOK. However, AO FSO systems are expensive and have large size, weight, and power consumption. More importantly, AO FSO systems still leave much to be desired in terms of reliability since AO does not provide perfect wavefront correction due to the limited throw, limited spatial resolution of the optics, and limited response time making such a system inadequate to follow rapid changes in turbulent conditions. As a result, the theoretical sensitivity limit is rarely achieved in practice. Since reliability is the key impediment to widespread adoption of FSO communication systems, it is highly desirable to develop alternative solutions to combat turbulence and improve FSO reliability.

A distorted wavefront is a superposition of the fundamental mode (Gaussian) and high-order modes (e.g. Hermite-Gaussian). If photons in all of the modes in a distorted wavefront are

detected and the photocurrent due to photons in every mode are summed up constructively, wave-front correction becomes dispensable. A multimode photodetector can readily detect photons in all of the modes in a distorted wavefront. However, sensitivity for the multimode photodetector will be thermal noise limited at 1000s photons/bit for OOK. Taking advantage of recent advances in SDM, we demonstrate a turbulence-tolerant FSO communication system using a few-mode pre-amplified receiver consisting of a few-mode EDFA and a multimode photodetector. In comparison with an FSO system using a single-mode preamplified receiver, our few-mode FSO system can achieve error-free transmission with a 6 dB advantage in power budget over a single-mode FSO system under the same conditions.

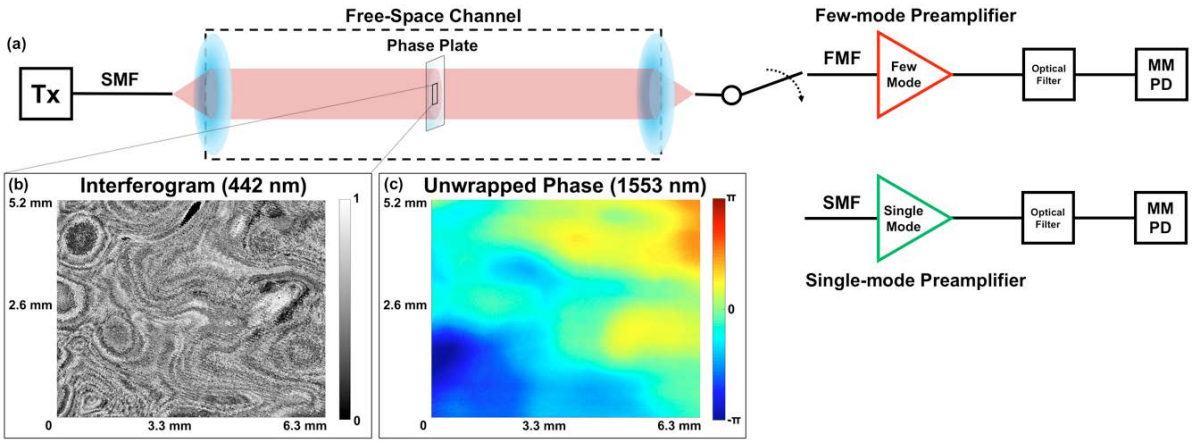

Figure 5.8 (a) Schematic of the FSO communication system including simulated atmospheric turbulence and the few-mode preamplifier. (b) Interferogram at 442 nm for phase retrieval. (c) Unwrapped phase at 1553nm derived from the interferogram.

A FSO communication system consists of a transmitter, the free-space channel and a receiver, as shown in Figure 5.8. In general, the free-space channel is turbulent as a result of spatial inhomogeneities in temperature and pressure, which lead to transverse and longitudinal variations of the refractive index. Instead of the conventional approach of using AO to correct wavefront distortion, our solution is to use a few-mode preamplified receiver to convert photons in all modes

into electrons. We used a 10-mode GI fiber to collect the light instead of a SMF. The collected signal is then amplified by a cladding-pumped few-mode amplifier before going to the multimode detector. We will present the details of the receiver and system performance in the next sections. Here we briefly describe how turbulence was generated in our experiments. For propagation distances within a few kilometers, intensity variation is typically much less than phase variation. Thus, turbulence can be simulated by a phase plate with appropriate randomness [86]. The strength of turbulence can be characterized by a phase structure function D(r), which describes the mean squared phase variations at different locations as defined by:

$$D(r) = \langle(\varphi(\overrightarrow{r'}) - \varphi(\overrightarrow{r'} + \vec{r}))^2\rangle \tag{6.12}$$

where φ denotes the local phase. In the sense of Kolmogorov turbulence [87,88], the phase structure function D is a function of the coherence length r_0:

$$D(r) = 6.88(r/r_0)^{5/3} \tag{6.13}$$

The wavenumber (k) spectral density is:

$$\Phi(k) = 0.023{r_0}^{-5/3}k^{-11/3} \tag{6.14}$$

We emulate such a phase variation in our experiment using phase plates created by repeatedly spray coating glass substrates. We measured the phase distribution using a phase-shifting interferometer, in which the optical path difference is achieved by applying different voltages to a liquid crystal cell. Figure 5.8 (b) shows one of the phase interferograms. The phase structure function can be calculated by Eq. (6.12). The Fried parameter is calculated to be 5 mm. The total wavefront distortion within the 6.3 mm aperture of the interferometer is approximately $\pm\pi$.

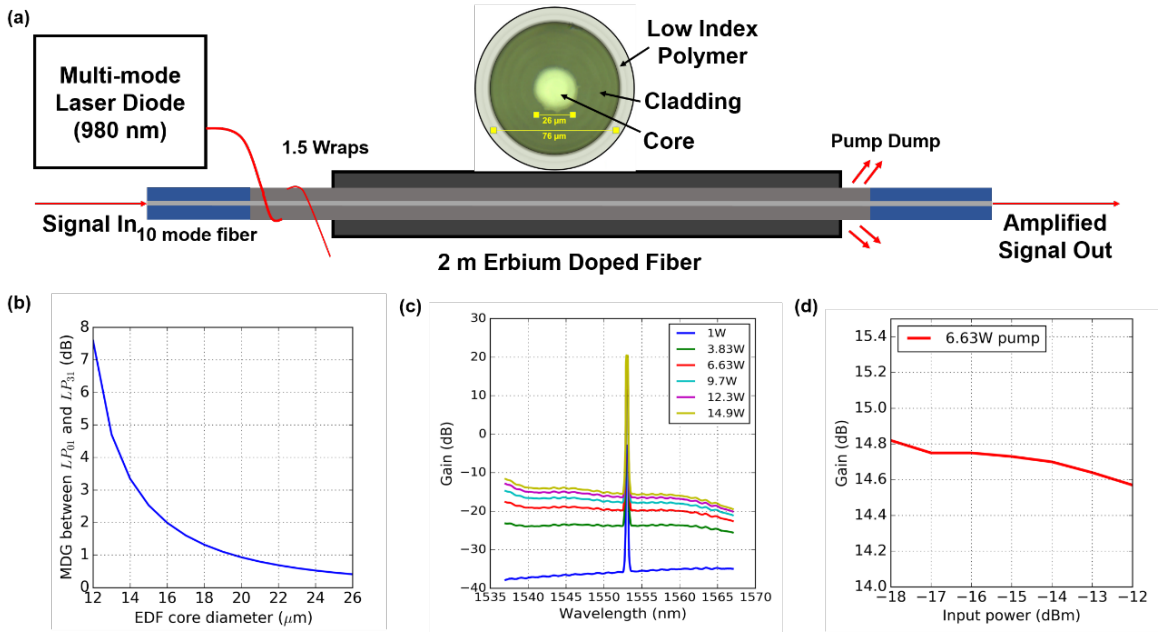

Figure 5.9 (a) Schematic of the few-mode EDFA. (b) MDG between the lowest (LP_{01}) and the highest-order mode (LP_{31}) vs EDF core diameter. (c) Gain characterization of the LP_{01} mode at different pump powers for an input power of -12 dBm. (d) Gain characterization of the LP_{01} mode at 1553nm with different input powers.

Low noise figure (NF) and low mode-dependent gain (MDG) of the few-mode amplifier is critical for the preamplified few mode receiver. Figure 5.9 (a) shows the schematic of the low MDG cladding pumped EDFA. A cladding-pumped few-mode amplifier with an EDF of core diameter 26 µm was built which can support 42 spatial modes. The few-mode Er-doped fiber has two cladding layers, an outer layer having lower refractive index and an inner cladding having higher refractive index. Pump light coming from a multi-mode laser diode (MMLD) is coupled into the inner cladding of the EDF through side pumping. To realize side pumping, we spliced the MMF pigtail of the MMLD to a coreless fiber and down tapered the coreless fiber from 125 µm to 20 µm with a tapered length of 30 mm. Then, the tapered coreless fiber was wrapped 1.5 turns around the 2m EDF. The small-signal gain is 10.5 dB/m. Since the intensity overlap of the 10 spatial modes of the input signal with the multimode pump is approximately the same, MDG is

greatly reduced. Our simulation in Figure 5.9 (b) shows that, when the EDF core diameter increases, the small-signal MDG can be reduced to less 0.5 dB. Figure 5.9 (c) and (d) show the gain characterization of the LP_{01} mode at different pump power and input power, respectively.

To evaluate the advantage of using few-mode preamplified receivers, phase plates representing various turbulence levels were generated based on Eq. (6.12), with each turbulence level having 500 statistically independent realizations. We simulate turbulence-induced power loss for both the 10-mode receiver (blue) and the single-mode receiver (red), as shown in Figure 5.10 (a). The term (d/r_0) on the x-axis is a measure of phase variation and d is the aperture size (1cm in this simulation). The average losses are represented by solid lines. The shaded region represents the power variation for different realizations of each turbulence condition. It is observed that the average loss and received power fluctuation for the10-mode receiver are much smaller than the single-mode receiver. Inclusion of more mode will improve the performance in this regard further.

However, the sensitivity of the few-mode preamplified OOK receiver decreases as the number of modes increases. This is because of the increase in the degrees of freedom of the spontaneous emission noise. Assuming that each mode has equal gain and noise figure, the few-mode preamplified receiver sensitivity as a function of the number of modes in the distorted wavefront is shown in Figure 5.10 (b). Fortunately, the sensitivity increases slowly as the number of modes increases, leading to a sensitivity penalty of only 1.2 dB (3 dB) when using 10 (50) modes.

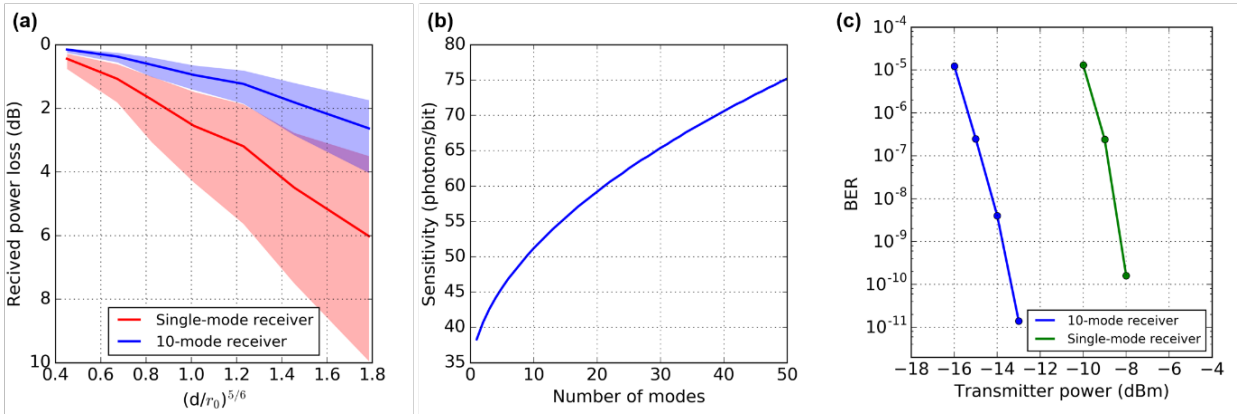

Figure 5.10 (a) Received power loss at different phase variations. (b) Sensitivity of few-mode preamplified OOK receiver as a function of the number of modes. (c) BERs for the 10-mode and single-mode preamplified receiver vs transmitter power.

In our transmission experiment, a 10 GHz OOK signal from a single-mode transmitter is expanded into a beam of diameter around 1 cm. With a coherence length of 5 mm, the phase variation across the beam is scaled by (d/r_0) to $\pm 2\pi$. The pump power for the few-mode amplifier is 6.63 W, which provides a ~15 dB gain shown in Figure 5.9 (d). The bit error rate (BER) was measured at different transmitter power levels as shown in Figure 5.10 (c). As a comparison, BERs using a single-mode preamplifier with the same gain were also measured. The comparison shows that the 10-mode preamplified receiver can provide a 6 dB increase in power budget over the single-mode preamplified receiver.

We take advantage of recent advances in space-division multiplexing to construct turbulence-resistant FSO communication systems. By converting the current single-mode preamplified receivers to few-mode preamplified receivers, we eliminate the complicated, expensive and sometime unreliable adaptive optics in FSO. A 6 dB increase in FSO link power budget was demonstrated in this experiment. The technique presented here can significantly expand the application

space for FSO communication. Also, the few-mode preamplified receivers can be used with AO systems for more severe environment or algorithm reduction.

CHAPTER 6: LONG-PERIOD GRATING FOR INTRODUCING STRONG MODE CROSSTALK

Another problem facing few mode fiber transmission system is the group delay spread at the reciver side. One way to mitigate it is to introduce strong mode coupling in the FMF [89]. One can simply insert a mode scrambler sandwiched between a pair of mode multiplexers. Another proposal is using long-period gratings (LPG) to achieve strong mode coupling between mode groups in GI FMFs [90–92]. LPG is a low-loss mode converter mediated by phase-matched mode coupling. It has been used for gain equalization [93], chromatic dispersion compensation [94] and sensors [95]. LPGs can be fabricated using UV exposure [96–102], CO_2 laser writing [103–109] or simply mechanical pressure [110–114]. The main drawback of using LPG directly written on GI transmission fiber for mode mixing is losses due to phase-matched output coupling of the modes of the highest mode group to lossy cladding modes.

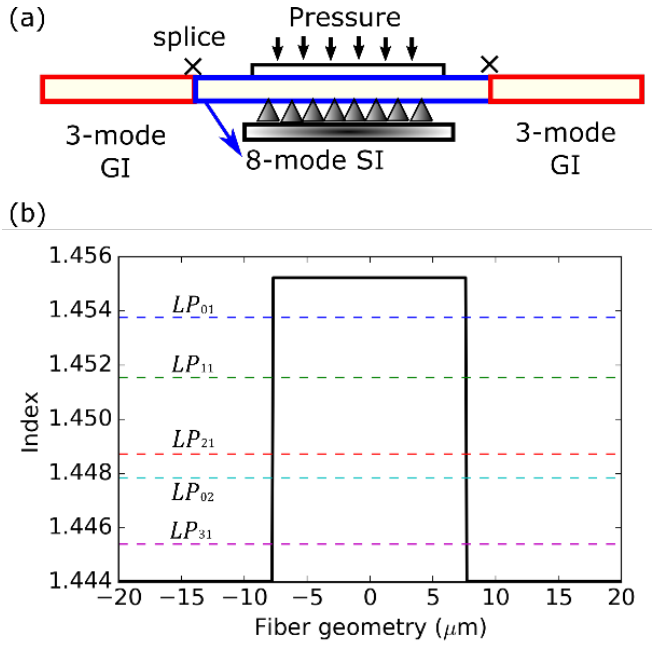

Figure 6.1 (a) The schematic of mechanical grating using 8 mode step index fiber (b) the effective index of spatial modes of 8-mode step index fiber.

Here we propose a new architecture of grating as a strong coupling device. We first show that such a loss could be avoided for 3-mode mixing if the LPG is installed on an 8-mode step-index (SI) FMF. The architecture for the mode mixing is shown in Figure 6.1(a) in which the 3-mode graded-index transmission fiber is spliced to an 8-mode SI FMF on which a LPG is installed. We show that LP_{11} modes in 8-mode SI FMF will not couple to higher order modes or cladding modes. Figure 6.1(b) shows the effective indexes of the modes of the 8-mode SI FMF. The effective index difference between the LP_{01} and LP_{11} modes is 2.21×10^{-3}. The effective index difference between the LP_{11} and LP_{21} modes is 2.83×10^{-3} and the effective index difference between the LP_{11} mode and all other modes is larger than 2.83×10^{-3}. As a result, an LPG phase matched between the LP_{01} and LP_{11} modes of the SI FMF is not phase matched for mode coupling between LP_{11} and any other modes. So signals of the LP_{01} and LP_{11} modes in transmission fibers cannot be coupled to the higher-order mode or cladding modes, thus ultra-low loss mode conversion can be achieved.

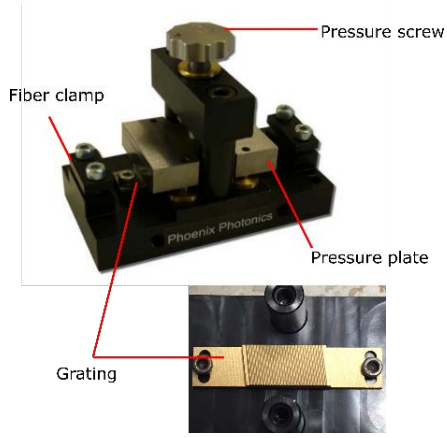

Figure 6.2 Image of the long period grating.

More generally, if the transmission fiber supports more than 3 modes, more gratings may be needed for the mode mixing since each grating is installed on the SI-FMF which has different effective index between the mode groups. Each grating is installed on a specially designed SI-FMF, which requires no resonant coupling from the transmission modes to the higher order modes or cladding modes. Such a design is in principle similar to 3-mode mixing case. Then by concatenating the gratings, mode mixing can be achieved. A possible drawback of the proposed approach is the splice loss between the designed SI-FMF and GI transmission fiber or one designed SI-FMF to another designed SI-FMF due to mode mismatch. The splice loss due to mode mismatch could, however, be largely suppressed by using intermediate fibers.

In experiment, we demonstrated mixing of three spatial modes in a GI transmission fiber using LPG on an eight-mode SI-FMF. Also, we fully characterized the coupling matrix characteristics of the grating for the first time. The LPG used in experiment is a pressure-induced mechanical grating, as shown in Figure 6.2. When a fiber is placed across the grating held by a clamp, a pressure can be exerted by the pressure screw through the flat pressure plate. A corresponding index perturbation is thus introduced through the elasto-optic effect. The grating period used is 710μm which is designed to match the index difference between the LP_{01} and LP_{11} modes in the SI-FMF. The phase-matching condition is given by:

$$n_{eff,01} - n_{eff,11} = \lambda/\Lambda \tag{8.1}$$

where $n_{\mathrm{eff},01}$ and $n_{\mathrm{eff},11}$ are the effective indexes of the LP_{01} and LP_{11} modes, λ is the wavelength and Λ is the grating period. The grating was attached to a base that allows adjustment of the angle between the fiber and the grating, and thus effective grating period or resonant wavelength.

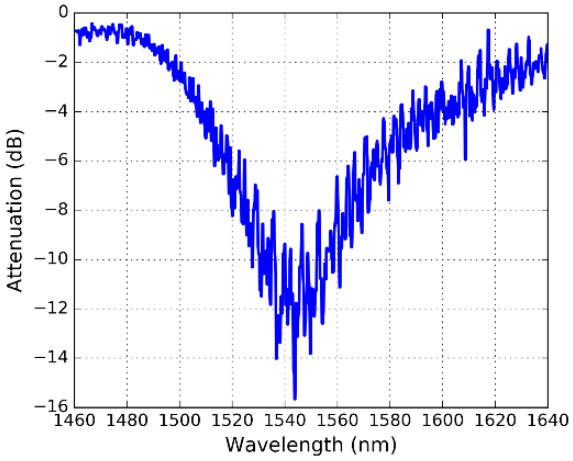

Figure 6.3 Spectrum response of the LP_{01} under the long period grating.

To characterize the LPG, we measured the transmission spectrum of the LPG using a broadband laser source and an optical spectrum analyzer (OSA). The SMF-pigtailed broadband laser source was center launched into the 8-mode SI FMF to predominantly excite the fundamental LP_{01} mode. At the output end, the 8-mode SI FMF is center spliced to the input SMF of the OSA Figure 6.3 shows the transmission spectrum of the LPG, which is optimally phase matched at 1542 nm. The 3-dB bandwidth for mode coupling is more than 80nm. This broad mode-coupling bandwidth is determined by the shape of each tooth of the LPG and the corresponding spatial frequency content of the index perturbation.

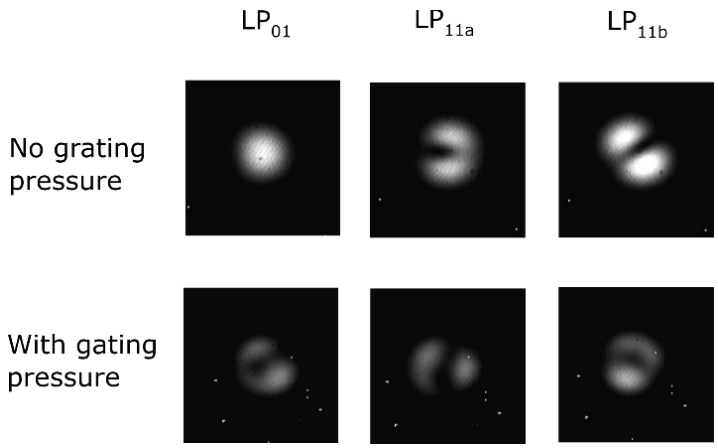

Figure 6.4 Mode intensity profile of each spatial mode without and with grating pressure.

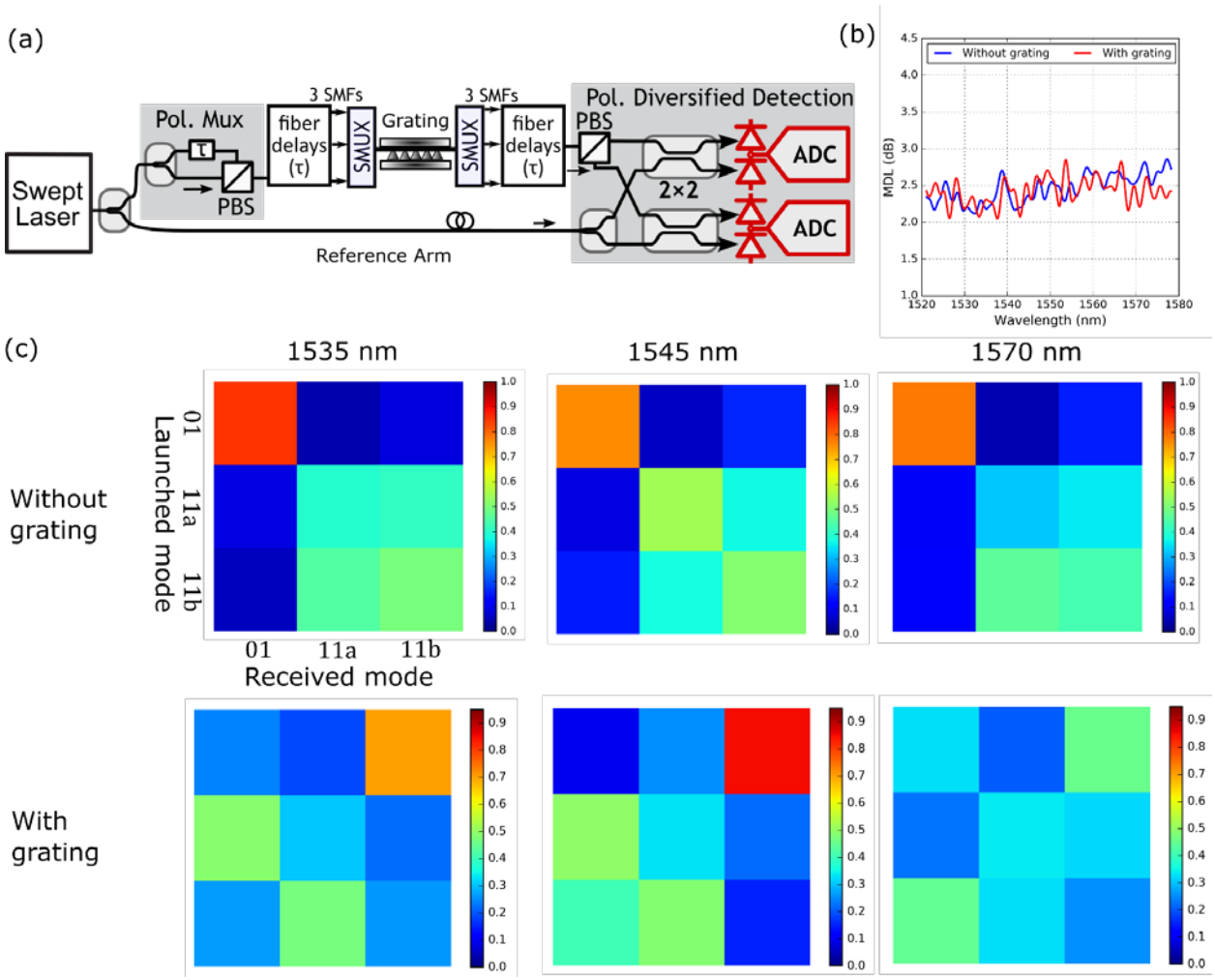

Figure 6.5 (a) Experimental setup for grating characterization. (b) MDL without and with grating vs wavelength (c) coupling matrix without and with grating at different wavelengths.

To characterize the mode-mixing performance, the two ends of the SI LPG were spliced to the 3-mode GI transmission fibers. The insertion loss (IL) was characterized by selectively exciting each spatial mode (LP_{01} or LP_{11}) using a mode-selective photonic lantern, which maps fundamental modes of input fibers to spatial modes of a FMF [xx]. Figure 6.4 shows the output (GI FMF-SI LPG-GI FMF) intensity profiles corresponding to each photonic lantern input fiber when (upper) no pressure is applied on the grating and (lower) when pressure is exerted on the grating. When no pressure is applied to the grating, the output is relatively pure LP mode. When pressure is exerted on the grating, the output becomes a mixture of the LP_{01} and LP_{11} modes, which is an evidence of strong coupling. When a pressure is applied to the LPG for strong mode mixing, the insertion loss was measured to be around 0.5 dB when each of the three modes was selectively excited. This loss includes the LPG and also the two splices from the SI FMF to the GI transmission fiber. Similar loss for selective excitations of the LP_{01} and LP_{11} modes is an indication of low MDL.

To characterize the MDL of the LPG, a pair of mode-selective photonic lanterns and a swept wavelength interferometer (SWI) were used. The experimental setup is shown in Figure 6.5(a). The SWI comprises a tunable laser source, a polarization multiplexer (Pol Mux), a fiber interferometer and a polarization-diversity coherent receiver. The receiver includes one polarization beam splitter (PBS), two 2 x 2 couplers, two balanced photodiodes and two 100-MS/s analog-to-digital converters. In the experiment, the swept-wavelength laser light was first split into the signal and reference arms of the interferometer. The signal light goes through the Pol Mux so that two orthogonal polarizations of equal power were generated. Fiber delays were added at the input and output of the pair of 3-mode photonic lanterns to differentiate the input-output response in the time domain. The LPG was inserted in between the two lanterns. The principle of operation of the SWI has been explained in previous chapter.The SWI can measure the 6x6 transfer matrix of the

system at each wavelength within the sweeping range. The 3x3 power transfer matrix between the total powers in both polarizations of output modes and those of the input mode can be readily derived from the 6x6 transfer matrix. MDL is defined as the ratio between the largest and smallest singular value of the transfer matrix. The transfer matrix of an ideal mode selective photonic lantern is unitary and block diagonal. Thus the MDL of the system is the same as the MDL of the grating. However, due to fabrication imperfections, especially the mode mismatch between the photonic lantern to the 3-mode GI, the transfer matrix without the LPG is not unitary. Since the transfer matrix of the photonic lanterns, even including the mode mismatch between the output fiber of FMF photonic lantern to the 3-mode GI transmission FMF, is quasi unitary, the MDL of the LPG can be estimated from two measurements. One measures the MDL of a pair of photonic lanterns and the other measures the pair of photonic lanterns plus the LPG inserted in between. The difference in MDL between these two measurements can be approximated as the MDL introduced by the LPG itself. Figure 6.5(b) shows the MDLs without (blue) and with (red) the LPG from 1520nm to 1580nm. The blue curve and the red curve almost overlap with each other, which means that the MDL the LPG is negligible. This result is in agreement with the loss measurements for the LP_{01} and LP_{11} mode presented earlier.

We next looked at the details of the power transfer matrix at different wavelengths, presented graphically in Figure 6.5 (c). The power transfer matrix without and with grating at three wavelengths within the C band are shown. The column shows the specific mode launched while the row shows the specific mode received, which forms the 3×3 power coupling matrix. Without grating, the power coupling matrix is almost block diagonal. More than 80% of the power of LP_{01} is received by LP_{01}, the LP_{11} behave in a similar fashion. When a pressure is applied on the grating, the power transfer matrix changes dramatically. We now observe large off-block diagonal terms

which represent strong coupling between the LP_{01} and LP_{11} modes. At 1535nm and 1545nm (1570nm), more than 90% (70%) of the power in the LP_{01} mode couples to the LP_{11} mode, which is in consistency with Fig. 3. Similarly, coupling from the two LP_{11} modes to the LP_{01} mode can be clearly observed. More than 70% of the power in the LP_{11} modes are coupled to the LP_{01} mode, which can be estimated by adding two power matrix elements: row 2 column 1 and row 3 column 1

In conclusion, we demonstrated strong mode mixing across large bandwidth for 3-spatial mode using long period mechanical grating on an 8 mode SI FMF with low IL and MDL.

LIST OF REFERENCES

1. C. A. Brackett, "Dense wavelength division multiplexing networks: principles and applications," IEEE J. Sel. Areas Commun. 8, 948–964 (1990).

2. R. W. Tkach, A. R. Chraplyvy, and R. M. Derosier, "Performance of a WDM network based on stimulated Brillouin scattering," IEEE Photonics Technol. Lett. 1, 111–113 (1989).

3. R. J. Mears, L. Reekie, I. M. Jauncey, and D. N. Payne, "Low-noise erbium-doped fibre amplifier operating at 1.54 μm," Electron. Lett. 23, 1026–1028 (1987).

4. E. Desurvire, J. R. Simpson, and P. C. Becker, "High-gain erbium-doped traveling-wave fiber amplifier," Opt. Lett. 12, 888–890 (1987).

5. M. Shimizu, M. Yamada, M. Horiguchi, T. Takeshita, and M. Okayasu, "Erbium-doped fibre amplifiers with an extremely high gain coefficient of 11.0 dB/mW," Electron. Lett. 26, 1641–1643 (1990).

6. D.-S. Ly-Gagnon, K. Katoh, and K. Kikuchi, "Unrepeated 210-km Transmission with Coherent Detection and Digital Signal Processing of 20-Gb/s QPSK Signal," in Optical Fiber Communication Conference and Exposition and The National Fiber Optic Engineers Conference (2005), Paper OTuL4 (Optical Society of America, 2005), p. OTuL4.

7. A. H. Gnauck, P. J. Winzer, C. R. Doerr, and L. L. Buhl, "10 x 112-Gb/s PDM 16-QAM transmission over 630 km of fiber with 6.2-b/s/Hz spectral efficiency," in 2009 Conference on Optical Fiber Communication - Incudes Post Deadline Papers (2009), pp. 1–3.

8. Y. Yamamoto, Y. Kawaguchi, and M. Hirano, "Low-Loss and Low-Nonlinearity Pure-Silica-Core Fiber for C- and L-band Broadband Transmission," J. Light. Technol. 34, 321–326 (2016).

9. D. a. Pinnow, T. c. Rich, F. w. Ostermayer, and M. DiDomenico, "Fundamental optical attenuation limits in the liquid and glassy state with application to fiber optical waveguide materials," Appl. Phys. Lett. 22, 527–529 (1973).

10. J.-X. Cai, Y. Cai, C. R. Davidson, D. G. Foursa, A. Lucero, O. Sinkin, W. Patterson, A. Pilipetskii, G. Mohs, and N. S. Bergano, "100-Gb/s undersea transmission with high spectral eff iciency using pre-filtered QPSK modulation format (Invited Paper)," Chin. Opt. Lett. 8, 831–836 (2010).

11. S. Randel, R. Ryf, A. Sierra, P. J. Winzer, A. H. Gnauck, C. A. Bolle, R.-J. Essiambre, D. W. Peckham, A. McCurdy, and R. Lingle, "6×56-Gb/s mode-division multiplexed transmission over 33-km few-mode fiber enabled by 6×6 MIMO equalization," Opt. Express 19, 16697–16707 (2011).

12. R. Ryf, H. Chen, N. K. Fontaine, A. M. Velázquez-Benítez, J. Antonio-López, C. Jin, B. Huang, M. Bigot-Astruc, D. Molin, F. Achten, P. Sillard, and R. Amezcua-Correa, "10-Mode mode-multiplexed transmission over 125-km single-span multimode fiber," in 2015 European Conference on Optical Communication (ECOC) (2015), pp. 1–3.

13. L. Grüner-Nielsen, Y. Sun, J. W. Nicholson, D. Jakobsen, K. G. Jespersen, J. Robert Lingle, and B. Pálsdóttir, "Few Mode Transmission Fiber With Low DGD, Low Mode Coupling, and Low Loss," J. Light. Technol. 30, 3693–3698 (2012).

14. N. Bai, E. Ip, Y.-K. Huang, E. Mateo, F. Yaman, M.-J. Li, S. Bickham, S. Ten, J. Liñares, C. Montero, V. Moreno, X. Prieto, V. Tse, K. M. Chung, A. P. T. Lau, H.-Y. Tam, C. Lu, Y. Luo, G.-D. Peng, G. Li, and T. Wang, "Mode-division multiplexed transmission with inline few-mode fiber amplifier," Opt. Express 20, 2668–2680 (2012).

15. M. Salsi, C. Koebele, D. Sperti, P. Tran, P. Brindel, H. Mardoyan, S. Bigo, A. Boutin, F. Verluise, P. Sillard, M. Bigot-Astruc, L. Provost, F. Cerou, and G. Charlet, "Transmission at 2x100Gb/s, over Two Modes of 40km-long Prototype Few-Mode Fiber, using LCOS based Mode Multiplexer and Demultiplexer," in Optical Fiber Communication Conference/National Fiber Optic Engineers Conference 2011 (2011), Paper PDPB9 (Optical Society of America, 2011), p. PDPB9.

16. C. Koebele, M. Salsi, D. Sperti, P. Tran, P. Brindel, H. Mardoyan, S. Bigo, A. Boutin, F. Verluise, P. Sillard, M. Astruc, L. Provost, F. Cerou, and G. Charlet, "Two mode transmission at 2x100Gb/s, over 40km-long prototype few-mode fiber, using LCOS-based programmable mode multiplexer and demultiplexer," Opt. Express 19, 16593–16600 (2011).

17. P. Sillard, D. Molin, M. Bigot-Astruc, H. Maerten, D. V. Ras, and F. Achten, "Low-DMGD 6-LP-mode fiber," in OFC 2014 (2014), pp. 1–3.

18. T. Mori, T. Sakamoto, M. Wada, T. Yamamoto, and F. Yamamoto, "Low DMD four LP mode transmission fiber for wide-band WDM-MIMO system," in 2013 Optical Fiber Communication Conference and Exposition and the National Fiber Optic Engineers Conference (OFC/NFOEC) (2013), pp. 1–3.

19. L. Grüner-Nielsen, Y. Sun, J. W. Nicholson, D. Jakobsen, K. G. Jespersen, J. Robert Lingle, and B. Pálsdóttir, "Few Mode Transmission Fiber With Low DGD, Low Mode Coupling, and Low Loss," J. Light. Technol. 30, 3693–3698 (2012).

20. B. Zhu, T. F. Taunay, M. F. Yan, J. M. Fini, M. Fishteyn, E. M. Monberg, and F. V. Dimarcello, "Seven-core multicore fiber transmissions for passive optical network," Opt. Express 18, 11117–11122 (2010).

21. A. Sano, H. Takara, T. Kobayashi, and Y. Miyamoto, "Crosstalk-Managed High Capacity Long Haul Multicore Fiber Transmission With Propagation-Direction Interleaving," J. Light. Technol. 32, 2771–2779 (2014).

22. H. Takara, H. Ono, Y. Abe, H. Masuda, K. Takenaga, S. Matsuo, H. Kubota, K. Shibahara, T. Kobayashi, and Y. Miaymoto, "1000-km 7-core fiber transmission of 10 x 96-Gb/s PDM-16QAM using Raman amplification with 6.5 W per fiber," Opt. Express 20, 10100–10105 (2012).

23. B. Zhu, T. F. Taunay, M. Fishteyn, X. Liu, S. Chandrasekhar, M. F. Yan, J. M. Fini, E. M. Monberg, and F. V. Dimarcello, "112-Tb/s Space-division multiplexed DWDM transmission with 14-b/s/Hz aggregate spectral efficiency over a 76.8-km seven-core fiber," Opt. Express 19, 16665–16671 (2011).

24. J. Sakaguchi, Y. Awaji, N. Wada, A. Kanno, T. Kawanishi, T. Hayashi, T. Taru, T. Kobayashi, and M. Watanabe, "109-Tb/s (7x97x172-Gb/s SDM/WDM/PDM) QPSK transmission through 16.8-km homogeneous multi-core fiber," in Optical Fiber Communication Conference/National Fiber Optic Engineers Conference 2011 (2011), Paper PDPB6 (Optical Society of America, 2011), p. PDPB6.

25. J. Sakaguchi, B. J. Puttnam, W. Klaus, Y. Awaji, N. Wada, A. Kanno, T. Kawanishi, K. Imamura, H. Inaba, K. Mukasa, R. Sugizaki, T. Kobayashi, and M. Watanabe, "19-core fiber transmission of 19x100x172-Gb/s SDM-WDM-PDM-QPSK signals at 305Tb/s," in Optical Fiber Communication Conference (2012), Paper PDP5C.1 (Optical Society of America, 2012), p. PDP5C.1.

26. B. J. Puttnam, R. S. Luís, W. Klaus, J. Sakaguchi, J. M. D. Mendinueta, Y. Awaji, N. Wada, Y. Tamura, T. Hayashi, M. Hirano, and J. Marciante, "2.15 Pb/s transmission using a 22 core homogeneous single-mode multi-core fiber and wideband optical comb," in 2015 European Conference on Optical Communication (ECOC) (2015), pp. 1–3.

27. R. G. H. van Uden, R. A. Correa, E. A. Lopez, F. M. Huijskens, C. Xia, G. Li, A. Schülzgen, H. de Waardt, A. M. J. Koonen, and C. M. Okonkwo, "Ultra-high-density spatial division multiplexing with a few-mode multicore fibre," Nat. Photonics 8, 865–870 (2014).

28. R. Ryf, N. K. Fontaine, M. Montoliu, S. Randel, S. H. Chang, H. Chen, S. Chandrasekhar, A. H. Gnauck, R. J. Essiambre, P. J. Winzer, T. Taru, T. Hayashi, and T. Sasaki, "Space-division multiplexed transmission over 3 #x00D7;3 coupled-core multicore fiber," in OFC 2014 (2014), pp. 1–3.

29. S. Randel, M. Magarini, R. Ryf, R. J. Essiambre, A. H. Gnauck, P. J. Winzer, T. Hayashi, T. Taru, and T. Sasaki, "MIMO-based signal processing of spatially multiplexed 112-Gb/s PDM-QPSK signals using strongly-coupled 3-core fiber," in 2011 37th European Conference and Exhibition on Optical Communication (2011), pp. 1–3.

30. R. Ryf, R. J. Essiambre, S. Randel, A. H. Gnauck, P. J. Winzer, T. Hayashi, T. Taru, and T. Sasaki, "MIMO-Based Crosstalk Suppression in Spatially Multiplexed 3$,times ,$56-Gb/s PDM-QPSK Signals for Strongly Coupled Three-Core Fiber," IEEE Photonics Technol. Lett. 23, 1469–1471 (2011).

31. R. Ryf, J. C. Alvarado, B. Huang, J. Antonio-Lopez, S. H. Chang, N. K. Fontaine, H. Chen, R. J. Essiambre, E. Burrows, R. Amezcua-Correa, T. Hayashi, Y. Tamura, T. Hasegawa, and T. Taru, "Long-Distance Transmission over Coupled-Core Multicore Fiber," in ECOC 2016 - Post Deadline Paper; 42nd European Conference on Optical Communication (2016), pp. 1–3.

32. R. Ryf, S. Randel, N. K. Fontaine, M. Montoliu, E. Burrows, S. Chandrasekhar, A. H. Gnauck, C. Xie, R.-J. Essiambre, P. Winzer, R. Delbue, P. Pupalaikis, A. Sureka, Y. Sun, L. Gruner-Nielsen, R. V. Jensen, and R. Lingle, "32-bit/s/Hz Spectral Efficiency WDM Transmission over 177-km Few-Mode Fiber," in Optical Fiber Communication Conference/National Fiber Optic Engineers Conference 2013 (2013), Paper PDP5A.1 (Optical Society of America, 2013), p. PDP5A.1.

33. N. Keil, D. Felipe, Z. Zhang, M. Kleinert, C. Zawadzki, W. Brinker, A. Polatynski, G. Irmscher, M. Möhrle, H.-G. Bach, and M. Schell, "Novel Integration Technologies for Disruptive Capacity Upgrade in Data Centre Systems," in Optical Fiber Communication Conference (2016), Paper Th3F.3 (Optical Society of America, 2016), p. Th3F.3.

34. B. Huang, N. K. Fontaine, H. Chen, J. Cang, R. Ryf, R. J. Essiambre, T. Nagashima, T. Sasaki, and T. Hayashi, "Minimizing the modal delay spread in coupled-core two-core fiber," in 2016 Conference on Lasers and Electro-Optics (CLEO) (2016), pp. 1–2.

35. R. A. Bergh, G. Kotler, and H. J. Shaw, "Single-mode fibre optic directional coupler," Electron. Lett. 16, 260–261 (1980).

36. E. a. J. Marcatili, "Dielectric Rectangular Waveguide and Directional Coupler for Integrated Optics," Bell Syst. Tech. J. 48, 2071–2102 (1969).

37. C. D. Poole, H. M. Presby, and J. P. Meester, "Two-mode fibre spatial-mode converter using periodic core deformation," Electron. Lett. 30, 1437–1438 (1994).

38. I. K. Hwang, S. H. Yun, and B. Y. Kim, "Long-period fiber gratings based on periodic microbends," Opt. Lett. 24, 1263–1265 (1999).

39. S. Ramachandran, Z. Wang, and M. Yan, "Bandwidth control of long-period grating-based mode converters in few-mode fibers," Opt. Lett. 27, 698–700 (2002).

40. S. Choi and K. Oh, "A new LP02 mode dispersion compensation scheme based on mode converter using hollow optical fiber," Opt. Commun. 222, 213–219 (2003).

41. S. Ramachandran, B. Mikkelsen, L. C. Cowsar, M. F. Yan, G. Raybon, L. Boivin, M. Fishteyn, W. A. Reed, P. Wisk, D. Brownlow, R. G. Huff, and L. Gruner-Nielsen, "All-fiber grating-based higher order mode dispersion compensator for broad-band compensation and 1000-km transmission at 40 Gb/s," IEEE Photonics Technol. Lett. 13, 632–634 (2001).

42. K. Y. Song, I. K. Hwang, S. H. Yun, and B. Y. Kim, "High performance fused-type mode-selective coupler using elliptical core two-mode fiber at 1550 nm," IEEE Photonics Technol. Lett. 14, 501–503 (2002).

43. S. G. Leon-Saval, A. Argyros, and J. Bland-Hawthorn, "Photonic lanterns: a study of light propagation in multimode to single-mode converters," Opt. Express 18, 8430–8439 (2010).

44. D. Noordegraaf, P. M. W. Skovgaard, M. D. Maack, J. Bland-Hawthorn, R. Haynes, and J. Lægsgaard, "Multi-mode to single-mode conversion in a 61 port Photonic Lantern," Opt. Express 18, 4673–4678 (2010).

45. S. G. Leon-Saval, N. K. Fontaine, J. R. Salazar-Gil, B. Ercan, R. Ryf, and J. Bland-Hawthorn, "Mode-selective photonic lanterns for space-division multiplexing," Opt. Express 22, 1036–1044 (2014).

46. N. K. Fontaine, S. G. Leon-Saval, R. Ryf, J. R. S. Gil, B. Ercan, and J. Bland-Hawthorn, "Mode-selective dissimilar fiber photonic-lantern spatial multiplexers for few-mode fiber," in 39th European Conference and Exhibition on Optical Communication (ECOC 2013) (2013), pp. 1–3.

47. D. Noordegraaf, P. M. W. Skovgaard, M. D. Nielsen, and J. Bland-Hawthorn, "Efficient multi-mode to single-mode coupling in a photonic lantern," Opt. Express 17, 1988–1994 (2009).

48. B. Huang, C. Xia, G. Matz, N. Bai, and G. Li, "Structured directional coupler pair for multiplexing of degenerate modes," in 2013 Optical Fiber Communication Conference and Exposition and the National Fiber Optic Engineers Conference (OFC/NFOEC) (2013), pp. 1–3.

49. N. K. Fontaine, R. Ryf, J. Bland-Hawthorn, and S. G. Leon-Saval, "Geometric requirements for photonic lanterns in space division multiplexing," Opt. Express 20, 27123–27132 (2012).

50. S. Yerolatsitis, I. Gris-Sánchez, and T. A. Birks, "Adiabatically-tapered fiber mode multiplexers," Opt. Express 22, 608–617 (2014).

51. A. M. Velazquez-Benitez, J. E. Antonio-Lopez, J. C. Alvarado-Zacarias, G. Lopez-Galmiche, P. Sillard, D. Van Ras, C. Okonkwo, H. Chen, R. Ryf, N. K. Fontaine, and R. Amezcua-Correa, "Scaling the fabrication of higher order photonic lanterns using microstructured preforms," in (IEEE, 2015), pp. 1–3.

52. B. Huang, B. Huang, J. C. A. Zacarias, J. C. A. Zacarias, N. K. Fontaine, H. Chen, R. Ryf, F. Poletti, J. R. Hayes, J. Antonio-Lopez, R. A. Correa, and G. Li, "10-Mode Photonic Lanterns Using Low-Index Micro-structured Drilling Preforms," in Optical Fiber Communication Conference (2017), Paper Tu3J.5 (Optical Society of America, 2017), p. Tu3J.5.

53. B. Huang, N. K. Fontaine, R. Ryf, B. Guan, S. G. Leon-Saval, R. Shubochkin, Y. Sun, R. Lingle, and G. Li, "All-fiber mode-group-selective photonic lantern using graded-index multimode fibers," Opt. Express 23, 224–234 (2015).

54. H. Wen, C. Xia, A. M. Velázquez-Benítez, N. Chand, J. E. Antonio-Lopez, B. Huang, H. Liu, H. Zheng, P. Sillard, X. Liu, F. Effenberger, R. Amezcua-Correa, and G. Li, "First Demonstration of Six-Mode PON Achieving a Record Gain of 4 dB in Upstream Transmission Loss Budget," J. Light. Technol. 34, 1990–1996 (2016).

55. C. Xia, N. Chand, A. M. Velázquez-Benítez, Z. Yang, X. Liu, J. E. Antonio-Lopez, H. Wen, B. Zhu, N. Zhao, F. Effenberger, R. Amezcua-Correa, and G. Li, "Time-division-multiplexed few-mode passive optical network," Opt. Express 23, 1151–1158 (2015).

56. C. Xia, A. M. Velázquez-Benítez, J. E. A. Lopez, W. He, A. Schülzgen, F. Effenburger, R. A. Correa, and G. Li, "TDMA Few-Mode Passive Optical Network," in Asia Communications and Photonics Conference 2014 (2014), Paper ATh2F.2 (Optical Society of America, 2014), p. ATh2F.2.

57. C. Xia, N. Chand, A. M. Velázquez-Benítez, X. Liu, J. E. A. Lopez, H. Wen, B. Zhu, F. Effenberger, R. Amezcua-Correa, and G. Li, "Demonstration of world's first few-mode GPON," in 2014 The European Conference on Optical Communication (ECOC) (2014), pp. 1–3.

58. N. K. Fontaine, R. Ryf, M. A. Mestre, B. Guan, X. Palou, S. Randel, Y. Sun, L. Gruner-Nielsen, R. V. Jensen, and R. Lingle, "Characterization of Space-Division Multiplexing Systems using a Swept-Wavelength Interferometer," in (OSA, 2013), p. OW1K.2.

59. B. Huang, H. Chen, N. K. Fontaine, C. Jin, K. Shang, R. Ryf, R.-J. Essiambre, B. Ung, Y. Messaddeq, S. LaRochelle, and G. Li, "Spatially and Spectrally Resolved Gain Characterization of Space-Division Multiplexing Amplifiers With Coherent Swept-Wavelength Reflectometry," J. Light. Technol. 35, 741–747 (2017).

60. S. Chandrasekhar, A. H. Gnauck, X. Liu, P. J. Winzer, Y. Pan, E. C. Burrows, T. F. Taunay, B. Zhu, M. Fishteyn, M. F. Yan, J. M. Fini, E. M. Monberg, and F. V. Dimarcello, "WDM/SDM transmission of 10 x 128-Gb/s PDM-QPSK over 2688-km 7-core fiber with a per-fiber net aggregate spectral-efficiency distance product of 40,320 km·b/s/Hz," Opt. Express 20, 706–711 (2012).

61. N. Bai, E. Ip, Y.-K. Huang, E. Mateo, F. Yaman, M.-J. Li, S. Bickham, S. Ten, J. Liñares, C. Montero, V. Moreno, X. Prieto, V. Tse, K. M. Chung, A. P. T. Lau, H.-Y. Tam, C. Lu, Y. Luo, G.-D. Peng, G. Li, and T. Wang, "Mode-division multiplexed transmission with inline few-mode fiber amplifier," Opt. Express 20, 2668–2680 (2012).

62. J. Sakaguchi, B. J. Puttnam, W. Klaus, Y. Awaji, N. Wada, A. Kanno, T. Kawanishi, K. Imamura, H. Inaba, K. Mukasa, R. Sugizaki, T. Kobayashi, and M. Watanabe, "305 Tb/s Space Division Multiplexed Transmission Using Homogeneous 19-Core Fiber," J. Light. Technol. 31, 554–562 (2013).

63. E. Ip, M. J. Li, K. Bennett, Y. K. Huang, A. Tanaka, A. Korolev, K. Koreshkov, W. Wood, E. Mateo, J. Hu, and Y. Yano, "146 #x03BB; #x00D7; 6 #x00D7; 19-Gbaud Wavelength-and

Mode-Division Multiplexed Transmission Over 10 #x00D7; 50-km Spans of Few-Mode Fiber With a Gain-Equalized Few-Mode EDFA," J. Light. Technol. 32, 790–797 (2014).

64. E. Ip, N. Bai, Y.-K. Huang, E. Mateo, F. Yaman, S. Bickham, H.-Y. Tam, C. Lu, M.-J. Li, S. Ten, A. P. T. Lau, V. Tse, G.-D. Peng, C. Montero, X. Prieto, and G. Li, "88x3x112-Gb/s WDM Transmission over 50-km of Three-Mode Fiber with Inline Multimode Fiber Amplifier," in 37th European Conference and Exposition on Optical Communications (2011), Paper Th.13.C.2 (Optical Society of America, 2011), p. Th.13.C.2.

65. V. a. J. M. Sleiffer, Y. Jung, V. Veljanovski, R. G. H. van Uden, M. Kuschnerov, H. Chen, B. Inan, L. G. Nielsen, Y. Sun, D. J. Richardson, S. U. Alam, F. Poletti, J. K. Sahu, A. Dhar, A. M. J. Koonen, B. Corbett, R. Winfield, A. D. Ellis, and H. de Waardt, "73.7 Tb/s (96 x 3 x 256-Gb/s) mode-division-multiplexed DP-16QAM transmission with inline MM-EDFA," Opt. Express 20, B428–B438 (2012).

66. E. Ip, N. Bai, Y.-K. Huang, E. Mateo, F. Yaman, M.-J. Li, S. Bickham, S. Ten, Y. Luo, G.-D. Peng, G. Li, T. Wang, J. Linares, C. Montero, and V. Moreno, "6x6 MIMO Transmission over 50+25+10 km Heterogeneous Spans of Few-Mode Fiber with Inline Erbium-Doped Fiber Amplifier," in Optical Fiber Communication Conference (2012), Paper OTu2C.4 (Optical Society of America, 2012), p. OTu2C.4.

67. M. Yoshida, T. Hirooka, and M. Nakazawa, "Low-loss and reflection-free fused type fan-out device for 7-core fiber based on a bundled structure," Opt. Express 25, 18817–18826 (2017).

68. M. Yoshida, T. Hirooka, and M. Nakazawa, "Fused type fan-out device for multi-core fiber based on bundled structure," in 2016 Optical Fiber Communications Conference and Exhibition (OFC) (2016), pp. 1–3.

69. H. Uemura, K. Takenaga, T. Ori, S. Matsuo, K. Saitoh, and M. Koshiba, "Fused taper type fan-in/fan-out device for multicore EDF," in 2013 18th OptoElectronics and Communications Conference Held Jointly with 2013 International Conference on Photonics in Switching (OECC/PS) (2013), pp. 1–2.

70. Y. Jeong, J. K. Sahu, D. N. Payne, and J. Nilsson, "Ytterbium-doped large-core fiber laser with 1 kW continuous-wave output power," in Advanced Solid-State Photonics (2004), Paper PDP13 (Optical Society of America, 2004), p. PDP13.

71. Y.-C. Jeong, A. J. Boyland, J. K. Sahu, S.-H. Chung, J. Nilsson, and D. N. Payne, "Multi-kilowatt Single-mode Ytterbium-doped Large-core Fiber Laser," J. Opt. Soc. Korea 13, 416–422 (2009).

72. H. Chen, C. Jin, B. Huang, N. K. Fontaine, R. Ryf, K. Shang, N. Grégoire, S. Morency, R.-J. Essiambre, G. Li, Y. Messaddeq, and S. LaRochelle, "Integrated cladding-pumped multicore few-mode erbium-doped fibre amplifier for space-division-multiplexed communications," Nat. Photonics 10, 529–533 (2016).

73. Y. Jung, E. L. Lim, Q. Kang, T. C. May-Smith, N. H. L. Wong, R. Standish, F. Poletti, J. K. Sahu, S. U. Alam, and D. J. Richardson, "Cladding pumped few-mode EDFA for mode division multiplexed transmission," Opt. Express 22, 29008–29013 (2014).

74. K. S. Abedin, T. F. Taunay, M. Fishteyn, D. J. DiGiovanni, V. R. Supradeepa, J. M. Fini, M. F. Yan, B. Zhu, E. M. Monberg, and F. V. Dimarcello, "Cladding-pumped erbium-doped multicore fiber amplifier," Opt. Express 20, 20191–20200 (2012).

75. M. Salsi, D. Peyrot, G. Charlet, S. Bigo, R. Ryf, N. K. Fontaine, M. A. Mestre, S. Randel, X. Palou, C. Bolle, B. Guan, G. L. Cocq, L. Bigot, and Y. Quiquempois, "A Six-Mode Erbium-Doped Fiber Amplifier," in European Conference and Exhibition on Optical Communication (2012), Paper Th.3.A.6 (Optical Society of America, 2012), p. Th.3.A.6.

76. N. Bai, E. Ip, T. Wang, and G. Li, "Multimode fiber amplifier with tunable modal gain using a reconfigurable multimode pump," Opt. Express 19, 16601–16611 (2011).

77. A. Hartog and M. Gold, "On the theory of backscattering in single-mode optical fibers," J. Light. Technol. 2, 76–82 (1984).

78. J. P. von der Weid, R. Passy, B. Huttner, O. Guinard, and N. Gisin, "High-resolution distributed-gain measurements in erbium-doped fibers," IEEE Photonics Technol. Lett. 10, 949–951 (1998).

79. M. Wegmuller, P. Oberson, O. Guinnard, B. Huttner, L. Guinnard, C. Vinegoni, and N. Gisin, "Distributed gain measurements in Er-doped fibers with high resolution and accuracy using an optical frequency domain reflectometer," J. Light. Technol. 18, 2127–2132 (2000).

80. N. K. Fontaine, R. Ryf, M. A. Mestre, B. Guan, X. Palou, S. Randel, Y. Sun, L. Gruner-Nielsen, R. V. Jensen, and R. Lingle, "Characterization of Space-Division Multiplexing Systems using a Swept-Wavelength Interferometer," in OFC (OSA, 2013), p. OW1K.2.

81. J. P. von der Weid, R. Passy, G. Mussi, and N. Gisin, "On the characterization of optical fiber network components with optical frequency domain reflectometry," J. Light. Technol. 15, 1131–1141 (1997).

82. J. E. Kaufmann, "Performance limits of high-rate space-to-ground optical communications through the turbulent atmospheric channel," in (International Society for Optics and Photonics, 1995), Vol. 2381, pp. 171–183.

83. V. A. Vilnrotter and M. Srinivasan, "Adaptive detector arrays for optical communications receivers," IEEE Trans. Commun. 50, 1091–1097 (2002).

84. M. M. Fernandez and V. A. Vilnrotter, "Coherent optical receiver for PPM signals received through atmospheric turbulence: performance analysis and preliminary experimental results," in (International Society for Optics and Photonics, 2004), Vol. 5338, pp. 151–163.

85. K. Kikuchi, "Coherent Detection of Phase-Shift Keying Signals Using Digital Carrier-Phase Estimation," in Optical Fiber Communication Conference and Exposition and The National Fiber Optic Engineers Conference (2006), Paper OTuI4 (Optical Society of America, 2006), p. OTuI4.

86. S. Thomas, "A simple turbulence simulator for adaptive optics," in (International Society for Optics and Photonics, 2004), Vol. 5490, pp. 766–774.

87. A. N. Kolmogorov, "The Local Structure of Turbulence in Incompressible Viscous Fluid for Very Large Reynolds Numbers," Proc. Math. Phys. Sci. 434, 9–13 (1991).

88. D. L. Fried, "Statistics of a Geometric Representation of Wavefront Distortion," JOSA 55, 1427–1435 (1965).

89. K. P. Ho and J. M. Kahn, "Statistics of Group Delays in Multimode Fiber With Strong Mode Coupling," J. Light. Technol. 29, 3119–3128 (2011).

90. J. Fang, A. Li, and W. Shieh, "Low-DMD few-mode fiber with distributed long-period grating," Opt. Lett. 40, 3937–3940 (2015).

91. D. Askarov and J. M. Kahn, "Long-Period Fiber Gratings for Mode Coupling in Mode-Division-Multiplexing Systems," J. Light. Technol. 33, 4032–4038 (2015).

92. H. Liu, H. Wen, H. Wen, R. A. Correa, P. Sillard, G. Li, and G. Li, "Reducing group delay spread in a 9-LP mode FMF using uniform long-period gratings," in Optical Fiber Communication Conference (2017), Paper Tu2J.5 (Optical Society of America, 2017), p. Tu2J.5.

93. A. M. Vengsarkar, N. S. Bergano, C. R. Davidson, J. R. Pedrazzani, J. B. Judkins, and P. J. Lemaire, "Long-period fiber-grating-based gain equalizers," Opt. Lett. 21, 336–338 (1996).

94. S. Ramachandran, S. Ghalmi, S. Chandrasekhar, I. Ryazansky, M. F. Yan, F. V. Dimarcello, W. A. Reed, and P. Wisk, "Tunable dispersion compensators utilizing higher order mode fibers," IEEE Photonics Technol. Lett. 15, 727–729 (2003).

95. A. D. Kersey, M. A. Davis, H. J. Patrick, M. LeBlanc, K. P. Koo, C. G. Askins, M. A. Putnam, and E. J. Friebele, "Fiber grating sensors," J. Light. Technol. 15, 1442–1463 (1997).

96. R. Kashyap, P. F. Mckee, and D. Armes, "UV written reflection grating structures in photosensitive optical fibres using phase-shifted phase masks," Electron. Lett. 30, 1977–1978 (1994).

97. B. Poumellec, P. Guénot, I. Riant, P. Sansonetti, P. Niay, P. Bernage, and J. F. Bayon, "UV induced densification during Bragg grating inscription in Ge:SiO2 preforms," Opt. Mater. 4, 441–449 (1995).

98. F. Bakhti, P. Sansonetti, C. Sinet, L. Gasca, L. Martineau, S. Lacroix, X. Daxhelet, and F. Gonthier, "Optical add/drop multiplexer based on UV-written Bragg grating in a fused 100% coupler," Electron. Lett. 33, 803–804 (1997).

99. R. M. Atkins and V. Mizrahi, "Observations of changes in UV absorption bands of singlemode germanosilicate core optical fibres on writing and thermally erasing refractive index gratings," Electron. Lett. 28, 1743–1744 (1992).

100. G. D. Emmerson, S. P. Watts, C. B. E. Gawith, V. Albanis, M. Ibsen, R. B. Williams, and P. G. R. Smith, "Fabrication of directly UV-written channel waveguides with simultaneously defined integral Bragg gratings," Electron. Lett. 38, 1531–1532 (2002).

101. K. O. Hill, B. Malo, F. Bilodeau, D. C. Johnson, and J. Albert, "Bragg gratings fabricated in monomode photosensitive optical fiber by UV exposure through a phase mask," Appl. Phys. Lett. 62, 1035–1037 (1993).

102. D. S. Starodubov, V. Grubsky, J. Feinberg, B. Kobrin, and S. Juma, "Bragg grating fabrication in germanosilicate fibers by use of near-UV light: a new pathway for refractive-index changes," Opt. Lett. 22, 1086–1088 (1997).

103. M. A. Ahmed, J. Schulz, A. Voss, O. Parriaux, J.-C. Pommier, and T. Graf, "Radially polarized 3kW beam from a CO2 laser with an intracavity resonant grating mirror," Opt. Lett. 32, 1824–1826 (2007).

104. Y. P. Wang and Y. J. Rao, "Long period fibre grating torsion sensor measuring twist rate and determining twist direction simultaneously," Electron. Lett. 40, 164–166 (2004).

105. D. D. Davis, T. K. Gaylord, E. N. Glytsis, S. G. Kosinski, S. C. Mettler, and A. M. Vengsarkar, "Long-period fibre grating fabrication with focused CO2 laser pulses," Electron. Lett. 34, 302–303 (1998).

106. Y. Wang, L. Xiao, D. N. Wang, and W. Jin, "In-fiber polarizer based on a long-period fiber grating written on photonic crystal fiber," Opt. Lett. 32, 1035–1037 (2007).

107. Y.-P. Wang, L. Xiao, D. N. Wang, and W. Jin, "Highly sensitive long-period fiber-grating strain sensor with low temperature sensitivity," Opt. Lett. 31, 3414–3416 (2006).

108. H. S. Ryu, Y. Park, S. T. Oh, Y. Chung, and D. Y. Kim, "Effect of asymmetric stress relaxation on the polarization-dependent transmission characteristics of a CO2 laser-written long-period fiber grating," Opt. Lett. 28, 155–157 (2003).

109. P. E. Powers, T. J. Kulp, and S. E. Bisson, "Continuous tuning of a continuous-wave periodically poled lithium niobate optical parametric oscillator by use of a fan-out grating design," Opt. Lett. 23, 159–161 (1998).

110. S. Savin, M. J. F. Digonnet, G. S. Kino, and H. J. Shaw, "Tunable mechanically induced long-period fiber gratings," Opt. Lett. 25, 710–712 (2000).

111. S. W. James and R. P. Tatam, "Optical fibre long-period grating sensors: characteristics and application," Meas. Sci. Technol. 14, R49 (2003).

112. G. Rego, J. R. A. Fernandes, J. L. Santos, H. M. Salgado, and P. V. S. Marques, "New technique to mechanically induce long-period fibre gratings," Opt. Commun. 220, 111–118 (2003).

113. G. M. Rego, H. M. Salgado, and J. L. Santos, "Interrogation of a Fiber Bragg Grating Using a Mechanically Induced Long-Period Fiber Grating," IEEE Sens. J. 6, 1592–1595 (2006).

114. C.-Y. Lin, L. A. Wang, and G.-W. Chern, "Corrugated Long-Period Fiber Gratings as Strain, Torsion, and Bending Sensors," J. Light. Technol. 19, 1159 (2001).